

End of Degree Thesis
Bachelor's Degree in Industrial Technology

**Modeling and Simulation of Photovoltaic
Plant Cables**

Author: Sergi Casases López

Director: Eduardo Prieto Araujo

José Montero Cassinello

Date: 09 2019



Escola Tècnica Superior
d'Enginyeria Industrial de Barcelona



ABSTRACT

The aim of this project is to study the influence and consequences of utilizing different lengths of medium voltage cables to couple the grid with each Voltage Source Converter from a given solar park.

In other words, by varying the distance between each VSC converter with the point of common coupling (PCC), as well as changing the length between the PCC itself and the grid, this project aims to evaluate the effects of these changes on the qd currents of each solar park's converter.

Finally, by understanding its effects, a series of recommendations will be given in order to ensure the safest use of each VSC converter.

INDEX

GLOSSARY	6
1. MOTIVATION	7
2. ENERGY PRODUCTION MIX EVOLUTION	8
3. PHOTOVOLTAIC POWER PLANT	11
4. FLAWS OF SOLAR POWER.	14
5. VOLTAGE SOURCE CONVERTER.....	16
5.1. INTRODUCTION	16
5.2. PULSE WIDTH MODULATION	17
5.3. VSC MODEL.....	18
5.4. TRANSFORMATIONS.....	18
5.4.1. Clarke Transformation.....	18
5.4.2. Park Transformation.....	19
5.5. INSTANTANEOUS POWER THEORY	21
5.6. CONTROL SCHEMATICS	21
5.6.1 Phase Locked Loop (PLL)	21
5.6.2. Current References Computation	22
5.6.3. Current Loop Control.....	22
5.6.4. Current references computation	25
6. SIMULINK's VSC MODEL	26
6.1. Phase Locked Loop	26
6.2. Reference computation.....	27
6.3. Current Control Loop	28
7. CABLES OF STUDY.....	29
8. SIMULATION.....	31
8.1. DESCRIPTION OF THE SYSTEM.....	31
8.2. DESCRIPTION OF THE PARAMETRIC SIMULATIONS	33
8.3. CABLE'S MODEL SELECTION	35
8.4. SIMULATION 1	37
8.5. SIMULATION 2	44
8.6. SIMULATION 3.....	50
9. CONCLUSION	55
10. ENVIRONMENTAL IMPACT	56

11. ECONOMIC STUDY.....57

12. BIBLIOGRAPHY.....58

GLOSSARY

PCC Point of Common Coupling

VSC Voltage Source Converter

PV Photovoltaic

DC Direct Current

AC Alternating Current

PWM Pulse Width Modulation

IGBT Insulated Gate Bipolar Transistor

1. MOTIVATION

In the following chapter a brief description of the energy market, especially focusing on renewable energies, will be made. In those pages it is explained the importance of renewable energies, the impact that they have had for the past years as well as the expected upswing that they will experience during the following decade. For this reason, carrying out a research on such a global and rising market was deemed both interesting and useful.

Moreover, not many studies have been made on the impact of using long cables to couple the VSC converters to the grid in the solar photovoltaic field.

PV plants tend to be built in the outskirts of a city or in the countryside. Logically, the most important factor considered when choosing the location of its construction it's the amount of solar irradiance per day on that given site. However, set locations may not dispose of large portions of constructible land, either due to an abrupt terrain or because other constructions may get in the way.

Due to this reason, the PV plant may very well need to be built as smaller groups PV arrays, with independent voltage source converters, connected by medium voltage cables to the point of common coupling.

As said above, this project studies the consequences of building different sets of PV arrays far away from each other.

2. ENERGY PRODUCTION MIX EVOLUTION

Although renewable energies have been used by mankind since thousands of years ago, around the beginning of the 19th century sources such as coal and other non-renewables started to gain importance due to its energy efficiency.

Starting in the 19th century and all the way through the 20th century, non-renewable sources such as fossil fuels or nuclear energy had the highest impact in the energy production market. The considerably higher energy conversion efficiency alongside the fewer technological difficulties in the energy conversion itself made of the non-renewables a great choice.

However, the difficulty of replacing by natural means the primary energy sources of a non-renewable process alongside the negative effects of the waste products from the energy conversion brought great concern to the community. Therefore, other methods of electricity obtention were considered. These were the cleaner but less efficient renewable sources, which involve wind power, hydropower, solar energy, geothermal energy and bioenergy. Since this project focuses on the study and simulation of photovoltaic cables under different working conditions, a brief description of a photovoltaic power plant, its parts and processes will be made in future chapters.

First, in order to understand the importance of photovoltaic plants and its increasing impact on the electricity production, a brief description of the energy market over the last years will be made.

As it can be seen in the following graph, facilitated by the International Energy Agency (IEA) [1], up until the 1990's non-renewable energy sources covered over 80% of the electricity production. However, both coal and oil started to experience a decline in consumption, and so did nuclear energy during the beginning of the 21st century. Natural gas, on the other hand, experienced an increase in production thanks to the use of biomethane, a green non-fossil fuel source of energy, which consists up to 90% of methane. Nonetheless, nowadays most of natural gas energy conversion is still used from the nonrenewable primary source. Moreover, nonrenewable energy resources such as wind, geothermal and solar have experienced massive growth since the beginning of the past decade.

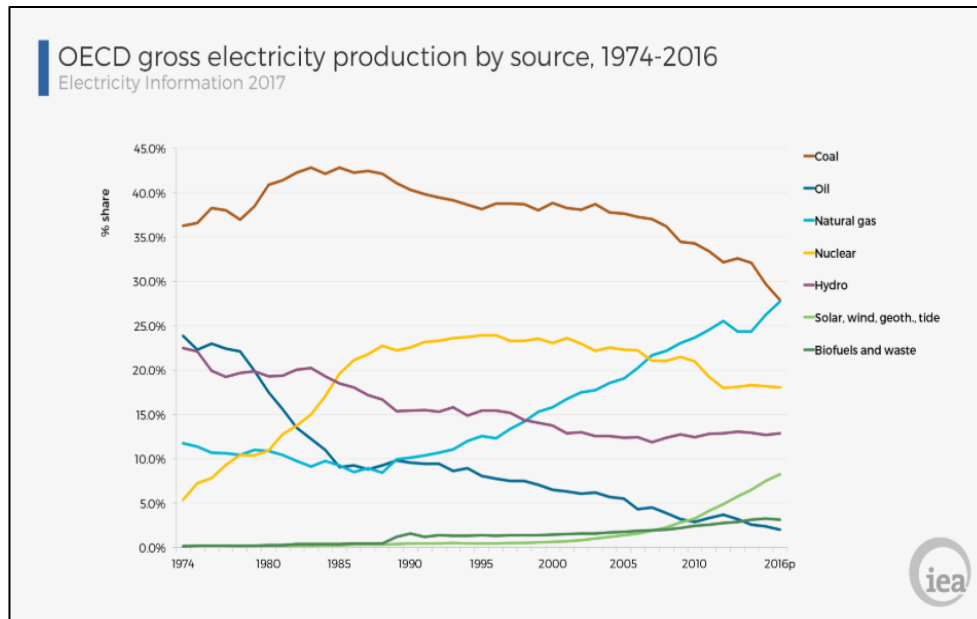


Figure 1: OECD gross electricity production by source [1].

To be more precise, between 2017 and 2018 there was a decrease in electricity production from fossil fuels, with declines from coal (-4,6 %) and oil (-9,0 %). However, electricity generation from renewable sources experienced significant growth, such as wind (+7,0 %) and solar (+19,8 %). These data were extracted from one of the International Energy Agency's data books [2].

It is important to state that these data were evaluated from OECD Countries, which consist of a group of nations who share about common eco-social problems. All of them form part of the so-called 1st world countries group and share a common sense of duty towards the reduction of emissions, waste products and primary sources. Moreover, being 1st world countries, they possess the technological knowledge and abilities to improve and exploit the renewables.

However, a global gross electricity production per source graph is shown below so that a more accurate view can be obtained.

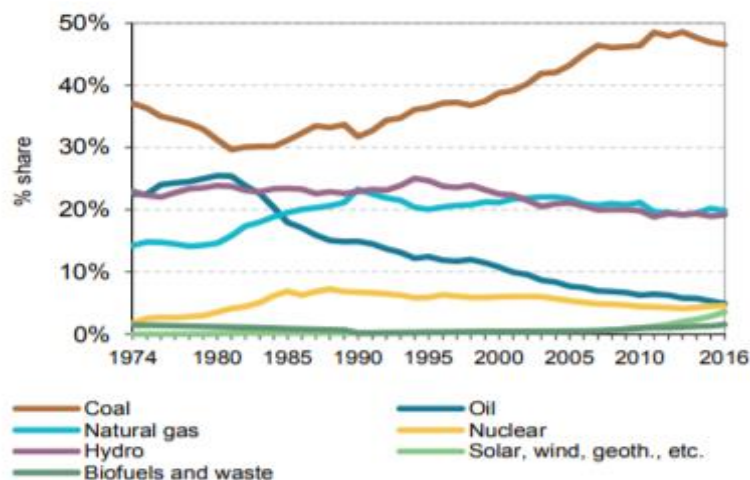


Figure 2: Global gross electricity production by source [1].

Nonetheless, renewables will have the most rapid growth in the electricity sector, providing almost 30% of power demand in 2023. During this five-year period (from 2018 to 2023), renewable resources are expected to meet more than 70% of global electricity generation growth, led by solar energy and followed by wind, hydropower and bioenergy. In terms of power capacity, hydropower continues to be the largest renewable source, meeting 16% of global electricity demand by 2023, followed by wind (6%), solar PV (4%) and bioenergy (3%) [3].

On the other hand, although growing at a slower pace than the power market, renewables in the heat sector are expected to show significant growth as well. Renewable heat consumption is expected to increase by 20% over the five-year period to end up covering an outstanding 12% ratio of the heating sector demand by 2023.

Renewables in transport have the lowest contribution of all three sectors, with their ratio growing only from 3.4% in 2017 to 3.8% in 2023.

As it is shown in the table above, solar energy is by far the renewable with a higher share increase. As explained in the previous chapter, this factor was key in order to develop this project.

Renewables	2017 (%)	2023 (%)	% Increase
Bioenergy	50	46	-8.00
Hydropower	31	27	-12.9
Wind	9	12	33.3
Solar	4	8	100
Solar thermal	4	4	0
Geothermal	2	3	50.0

Table 1: Representation of the expected increases by renewable source [3].

3. PHOTOVOLTAIC POWER PLANT

In this chapter a brief description of the main components of a PV plant will be made. In a typical photovoltaic power plant, the electricity generated goes through a series of transformations before it reaches the grid. Some examples of these transformations include power storage, DC-AC conversion, voltage adjustments, etc. A PV power plant, in order to ensure it can carry out safely and efficiently each one of these tasks, must have a specific series of components.

The typical energy transformation path in a grid connected PV system is as follows:

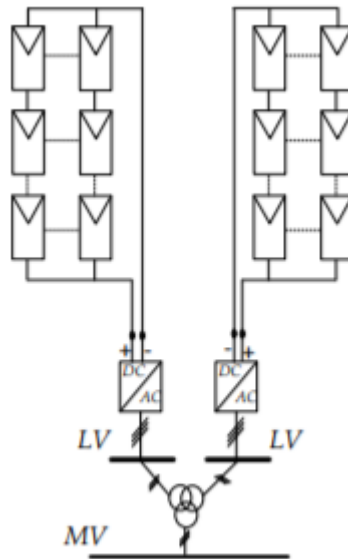


Figure 3: Energy path in a grid connected PV system [4].

A brief description of each component in this diagram will be now made.

- PV modules:

Photovoltaic power plants use large areas of photovoltaic cells, known as solar cells, to convert sunlight into electricity. These cells are usually made from silicon alloys. These solar panels tend to generate DC current voltages up to 1500 V and come in various forms:

- Crystalline solar panels: As the name suggests, these types of panels are made from crystalline silicon. They can be either monocrystalline or polycrystalline. Monocrystalline variants are more efficient (about 15-20%) but more expensive than polycrystallines (typically between 13-16% efficient) [5].

- Thin-film solar panels: A series of films are placed so that light is absorbed in different parts of the EM spectrum.

- Inverters:

Inverters are the components that convert DC power coming from the solar panels to AC power, which is necessary for the grid. To be more precise, inverters convert DC power into 60 or 50 Hz AC power. The use of inverters results in energy losses due to interferences. Typically, the losses obtained from a good quality inverter are around 10%.

Inverters are key components in both grid-connected and distributed power applications and are usually a significant part of the total system cost. The output current can be presented in different shapes, the most common being square waves, modified square waves and sine waves. Logically, the latter comes with the highest efficiency ratio. However, it's also highly expensive when compared to the other two. The modified square wave stands in the middle of the scale in both efficiency and cost. Finally, the square wave presents both values in both efficiency and cost.

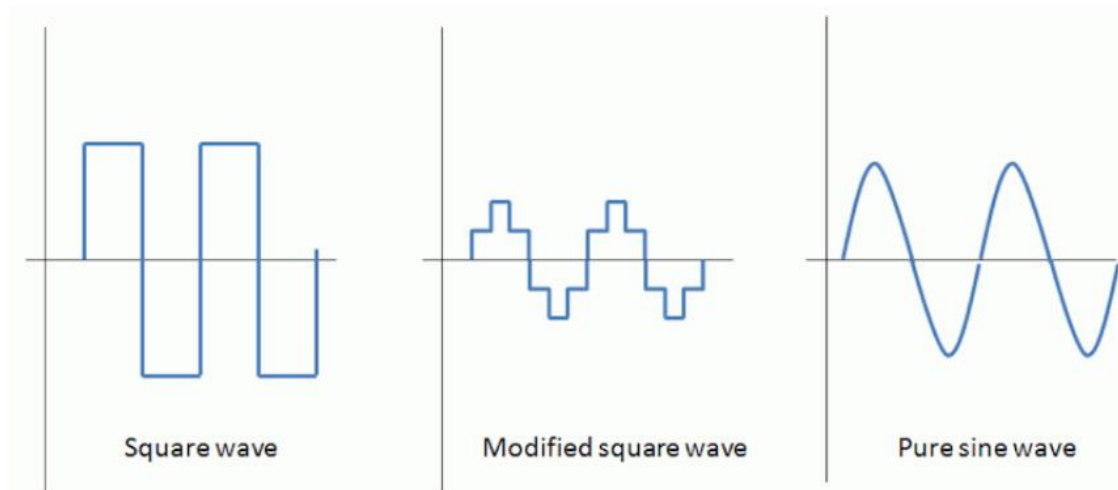


Figure 4: Representation of three common output wave forms [6].

Nowadays, most inverters convert DC power to AC power which is in synchronization with the grid. This proves very useful because if the grid should fail due to an unexpected event, the inverter will stop working as well.

Finally, it is important to know that there may be two steps of conversion. Instead of using one single stage to transform dc to ac, there might be one dc-dc converter and one dc-ac converter. Anyway, whatever method of conversion is used, inverters must deal with problems related to the PV panels and electrical requirements [4].

- Transformers:

As for transformers, they are used to increase or lower voltage of AC current. However, transformers always have losses, although good quality transformers present efficiency ratios that go as high as 95 %.

Other than the components described above, PV plants contain a large amount of supporting equipment, which serves to balance the system and to make it operational. The extra devices include wiring, connector boxes, switches, monitoring devices, etc. all of which help prepare electric power for utilization. It is interesting to underline that PV systems design are usually modular, which means that additional sections can be added to the plant or removed for repairs without significant disruption.

4. FLAWS OF SOLAR POWER.

In this chapter the two main problems or drawbacks regarding photovoltaic energy will be discussed. It is deemed important to outline its flaws in order to better understand their current position in the energy market. As for photovoltaic energy, their main drawbacks are as follow:

- One of the main drawbacks of photovoltaic energy is its intermittency. Solar energy is highly affected by non-controllable external factors such as bad weather or the night itself. The amount of cloud coverage and density has a big impact on solar to electricity conversion, therefore energy production greatly varies from season to season and from place to place.
- Solar cell efficiency: this factor refers to the portion of solar energy converted to electricity. Compared to other primary sources or electricity conversion methods, photovoltaic conversion is still far behind in terms of efficiency.

To see where current solar cells stand, a series of theoretical calculations shall now be explained. If one had a solar panel under ambient earth conditions (300 K) surrounded by an environment at 6000 K (temperature of the sun) the conversion ratio obtained through the Carnot Heat Engine expression $1 - \frac{T_c}{T_s}$ is 95%. However, when the panel's radiation emitted due to its temperature (higher than 0 K) is taken into account and subtracted from the net balance, the ratio drops to 86%. Furthermore, when the solar radiation comes from an area the size of the sun the ratio ends up dropping to 69% [7].

On the other hand, normal solar panels consist only of one p-n junction, which lowers its efficiency. In terms of electron-hole pairs and electricity conversion, some photons absorbed by the cell do not reach the material's minimum energy level (band gap) and is inevitably converted to heat. The photons which do surpass the band gap energy levels do end up forming electron-hole pairs, however only a portion of this energy is transformed into electricity. Keeping all these facts in mind it is proven that the efficiency ratio drops to a value of 33%.

Lastly, these 33% PV cells are still under study and are extremely expensive. Typical conversion ratios, as explained in the previous chapter, are around 16%.

In the following page a graph showing timeline of conversion ratios evolution is shown to better comprehend, on one hand, the great improvements made by scientists and on the other to show that there is still a long journey to make.

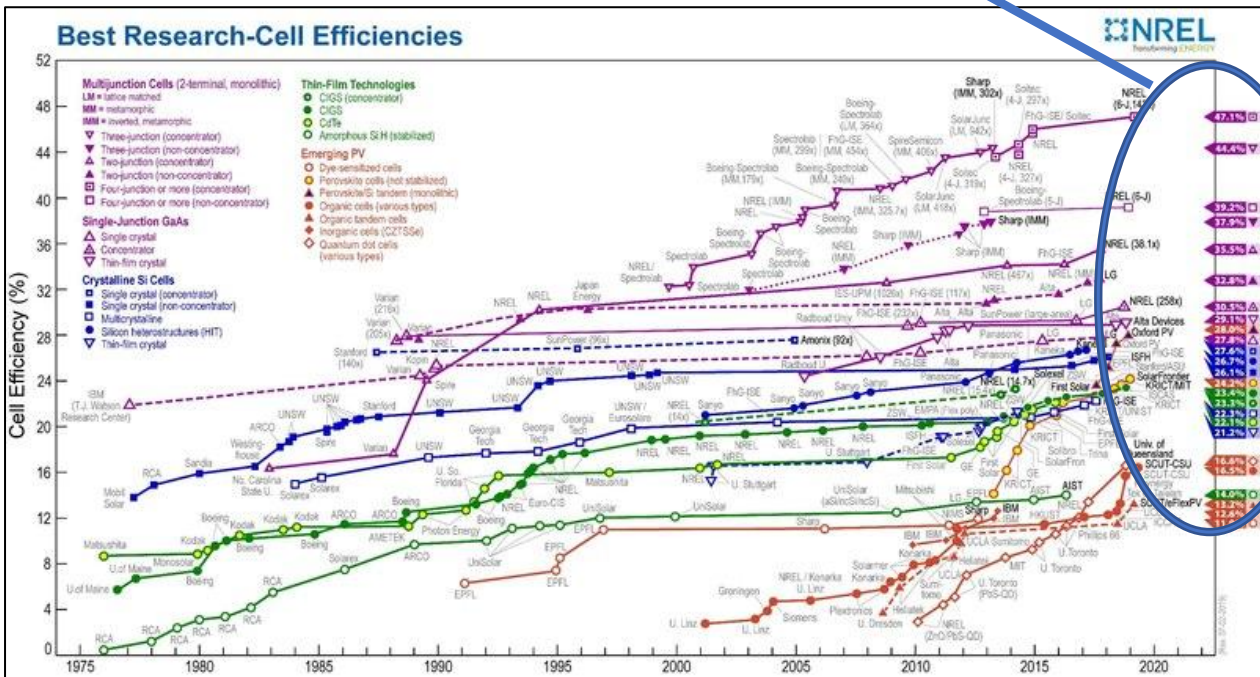
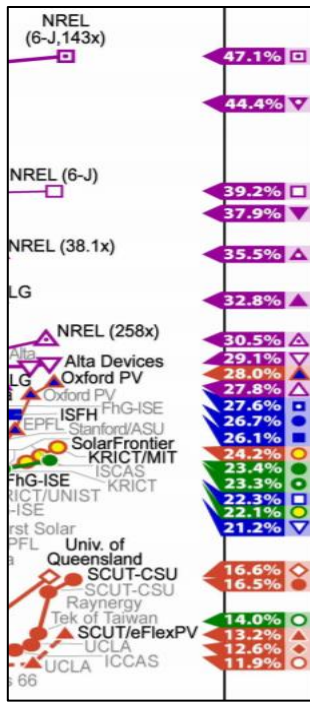


Figure 5: Timeline of solar cell conversion efficiencies research [7].

5. VOLTAGE SOURCE CONVERTER

Power electronics is an extremely important component in smart grids and renewable energy systems. It uses high switching devices to convert electrical power from ac-ac, ac-dc, dc-dc and dc-ac while being in control of the electric energy. This transformation is carried out by the converters.

In this chapter both the theory and the equations used to model in Simulink (Matlab) the VSC converters will be presented.

5.1. INTRODUCTION

In photovoltaic systems, DC-AC converters are needed in order to inject the generated power into the grid. A wide variety of converter topologies exist, however, in this project the two-level Voltage Source Converter, based on Insulated-Gate Bipolar Transistors, is the one that has been used.

Firstly, a brief description of a VSC will be made. Basically, a VSC generates AC voltage from a DC voltage. Although it is sometimes known as an inverter, it has the ability to transfer power in either direction. With a VSC, the magnitude, phase and frequency of the output voltage can be controlled. The DC side is accompanied by a capacitor, which must be large enough to endure the charge and discharge currents that flow through the system during the switching of the valves without greatly affecting the DC voltage, which should remain constant. As to the AC side, it is formed by the output voltage, the grid voltage and an inductor that acts both as a low-pass filter and a connection path between voltages.

An image describing the VSC in question is showed below.

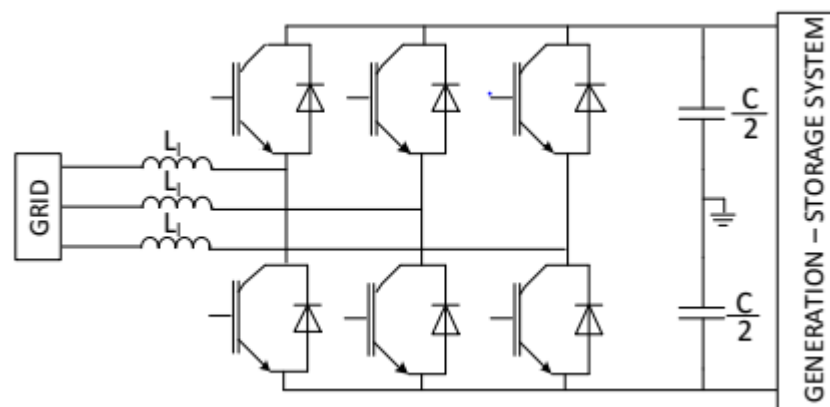


Figure 6: System description, involving the VSC converter and the grid [8].

5.2. PULSE WIDTH MODULATION

The main objective of the two-level VSC or any other topology is to apply a PWM-based voltage which can later be assimilated to a sinusoidal voltage, after an adequate filtering process (using inductor filters for example). This technique takes advantage of high switching frequency components such as the IGBT's. By switching very fast between two fixed voltages on the DC side ($\pm \frac{U_d}{2}$) and with the adequate low-pass filtering process, the desired sinusoidal voltage wave is obtained.

The filtering process is of great importance as not only it is necessary to achieve the desired wave form, but also to avoid injecting high frequency harmonics created by the PWM technique into the grid. Moreover, as mentioned above, the inductors also act as a current path that interconnects the voltages of the converter's AC side with the grid.

Finally, it is important to state that with PWM it is possible to create almost any phase, angle or amplitude by changing the PWM pattern. A way of changing this pattern would be to remain more time in the positive DC voltages than in the negative, through an adequate use of the IGBT's.

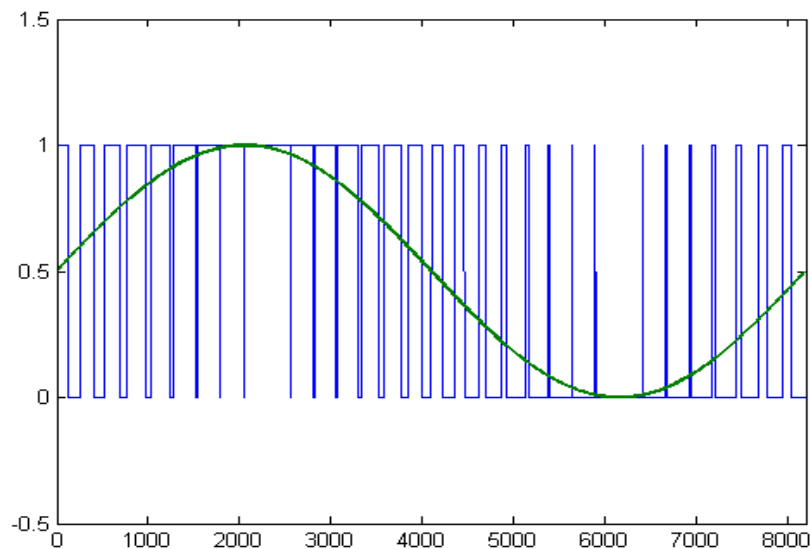


Figure 7: Representation of a PWM wave.

The main advantage of a VSC is that it enables the control of two electrical variables in order to separately control active and reactive power. In other words, the converter tells us which voltages need to be applied in order to control the currents that affect the active and reactive power in the system. The control structure of a VSC is constantly operating over time, with all the blocks adapting to changes in the grid and updating its values.

5.3. VSC MODEL

A schematic figure of the initial VSC modelled in this project is shown below. The AC side was modelled as three controlled voltage sources while the DC side has been removed in order to simplify the system at hand.

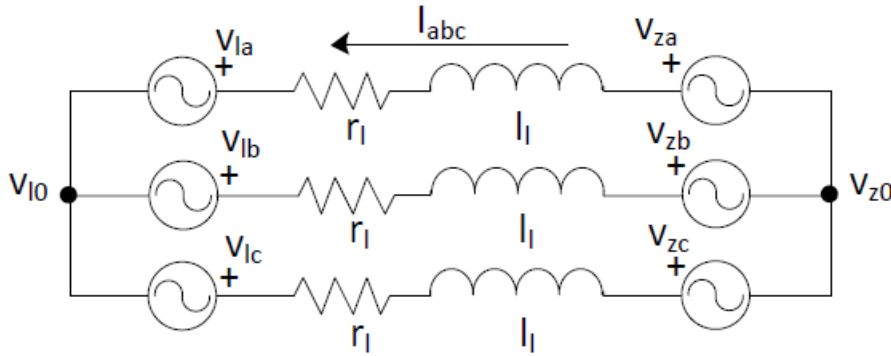


Figure 8: Simplified version of the system, comprising the grid and the AC side of the VSC converter [8].

In the figure above r_l is the inductance equivalent resistance while L_l is the inductance value. It is important to state that although there is no physical resistance between the grid and the VSC, they must be modelled as the inductance's present parasitic resistances.

As stated before, the VSC's AC side has modelled as three controlled voltage sources (V_i). Therefore, the grid is modelled as the three remaining voltage sources.

5.4. TRANSFORMATIONS

In order to simplify calculations, most systems work with a simplification of the three-phase voltage waves. The aim of this simplification is to cancel out the oscillatory effects of the system to end up obtaining a constant voltage, therefore facilitating the control schemes and calculations.

In order to understand the following chapters, a brief explanation on the theory behind these transformations will be made.

5.4.1. Clarke Transformation

The first step towards achieving constant voltages is the Clarke transformation, which transforms sinusoidal three-phase signals (120° phase shift between phases) into two sinusoidal signals (90° phase shift between phases). With Clarke the sinusoidal effect is not cancelled out. The main objective of this transformation is to achieve a change of

reference. This new reference allows us to orientate the signals so that instead of three variables we end up with two. It is defined as:

$$[x_{\alpha\beta 0}] = [T_{\alpha\beta 0}][x_{abc}] \quad (1)$$

where x_{abc} is the vector with the three-phase variables while $x_{\alpha\beta 0}$ is the vector with transformed variables in the $\alpha\beta 0$ domain. The transformation matrix is as follows:

$$T_{\alpha\beta} = \frac{2}{3} \begin{bmatrix} 1 & -\frac{1}{2} & -\frac{1}{2} \\ 0 & \frac{\sqrt{3}}{2} & \frac{\sqrt{3}}{2} \\ \frac{1}{2} & \frac{1}{2} & \frac{1}{2} \end{bmatrix} \quad (2)$$

Logically, this transformation is bidirectional. Therefore, all quantities in the $\alpha\beta 0$ domain can be transformed back to the three-phase domain.

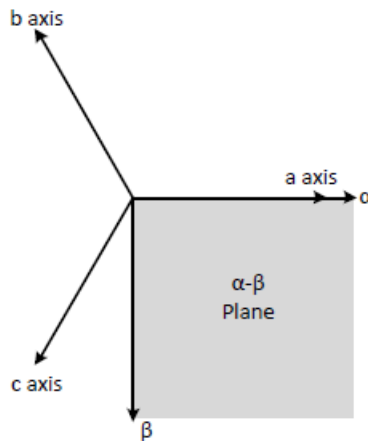


Figure 9: $\alpha\beta$ plane representation [8].

5.4.2. Park Transformation

The next step of Clarke Transformation is Park Transformation which includes an angle rotation (Θ). This allows us to express sinusoidal magnitudes as constant ones by rotating the $\alpha\beta$ planes shown in Figure 8. The park transformation is defined as:

$$[x_{qdo}] = [T_{qdo}][x_{abc}] \quad (3)$$

where x_{abc} is the vector with the three-phase variables while x_{qd0} stands for the vector in the $qd0$ domain. The transformation matrix can be defined as:

$$T(\theta) = \frac{2}{3} \begin{bmatrix} \cos(\theta) & \cos(\theta - \frac{2}{3}) & \cos(\theta + \frac{2}{3}) \\ \sin(\theta) & \sin(\theta - \frac{2}{3}) & \sin(\theta + \frac{2}{3}) \\ \frac{1}{2} & \frac{1}{2} & \frac{1}{2} \end{bmatrix} \quad (4)$$

The following figure illustrates the mentioned rotation applied to the Clarke transformation.

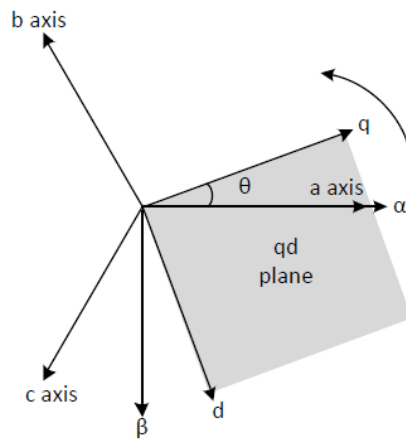


Figure 10: dq plane representation [8].

To easier visualize the effects of the Park Transformation on a three-phased quantity the following figure is presented.

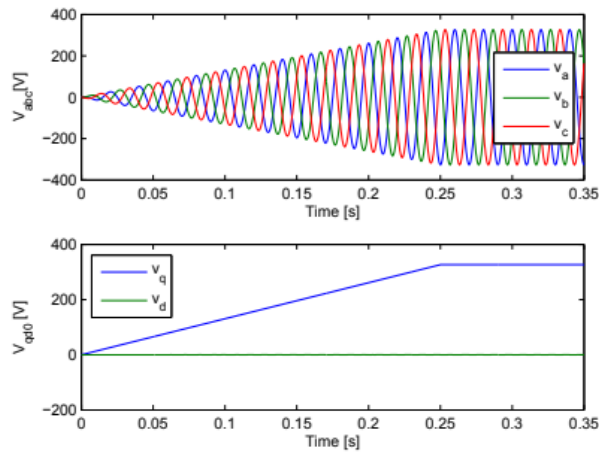


Figure 11: Example of three-phase voltages and consequent qd magnitudes [8].

5.5. INSTANTANEOUS POWER THEORY

It relates the active and reactive power with the voltages and currents in the $qd0$ domain. As q and d variables are constant its calculation is simple.

It is important to keep in mind that if the PLL is adequately synchronized with the system, it can be assumed that the V_{zd} component of the grid is zero. The final expressions are as follows:

$$P = \frac{3}{2} v_q i_q \quad (5)$$

$$Q = \frac{3}{2} v_q i_d \quad (6)$$

5.6. CONTROL SCHEMATICS

In order to appropriately control active and reactive power in an independent manner, the adequate control components need to be implemented.

5.6.1 Phase Locked Loop (PLL)

It is a tracking system which determines the phase voltage of the network. Its main objective is to track the grid angle. The PLL also gives us the frequency of the network as there is a derivative relationship between ω and Θ .

Moreover, in this control component we obtain the qd voltages, which, as stated before, represent a simplification of the three-phase voltage waves.

As for the parts of the PLL, there are three:

- Voltage measurement.
- Park Transformation.
- PLL controller.

As mentioned above, the PLL's main objective is to find the grid angle. To do so, the voltages must be oriented with a reference plane. Therefore, if we are orienting with the q plane, we want the d plane to be zero. As a result, a comparison with a constant zero is made as it is shown in the image below. Because the result of this comparison, the error, will be a constant magnitude, a simple PI controller can be used to track this difference. The PI controller will affect the frequency of our frame. This means that it will make our frame go slower or faster so that it matches the speed of our vector. The PI controller can be defined as:

$$K_f(s) = K_p \left(\frac{1 + s T_{PLL}}{s} \right) \quad (7)$$

As for K_p and τ_{PLL} can be obtained by solving the following system [8]:

$$\omega_n = \sqrt{\frac{K_p E_m}{\tau_{PLL}}} \quad (8)$$

$$\zeta = \frac{\sqrt{\tau_{PLL} K_p E_m}}{2} \quad (9)$$

Once the frequency of the rotation of our frame is calculated (ω), we integrate this variable in order to obtain the grid estimated angle (Θ). This is the angle that is going to be used for all the transformations in the control system.

Finally, it is important to state that the PLL is usually the first component to be started as it would be difficult to control the currents as well as the active and reactive power without knowing the voltage of the network.

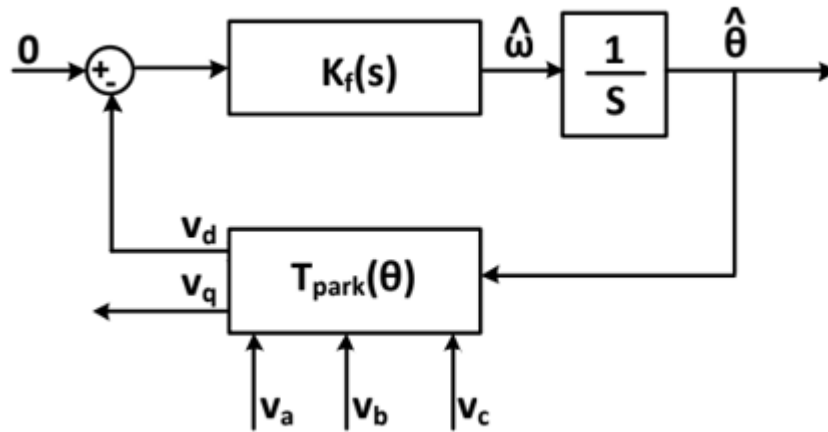


Figure 12: Representation of a PLL system [8].

5.6.2. Current References Computation

By receiving P^* and Q^* from the system (as the DC side has been neglected, these two outputs will be set to a given value) i_q^* and i_d^* current references are calculated thanks to the instantaneous power theory and the voltage of the network that the PLL calculates.

By measuring the currents from the feedback and transforming them, thanks to the grid angle calculated by the PLL, into magnitudes in the $qd0$ domain, they are compared with the current references mentioned above.

5.6.3. Current Loop Control

The current loop controls the regulation of the current that flows in the three-phase system, achieving the desired active and reactive power. This component can work either in the abc , $\alpha\beta 0$ or $qd0$ domains. However, in order to keep things simple, the $qd0$

domain is the one that has been used. It is also important to specify that the current loop operates at a defined time domain, which means the speed at which this component works can be specified.

In this $qd0$ domain two different trackers exist, one for the active current and the other for the reactive current. The starting point of the following equations can be concluded from Figure 8.

The equations of the system in a compact form (without neutral) and represented in a matricidal form are as follow:

$$v_{zabc} - v_{labc} = \begin{bmatrix} r_l & 0 & 0 \\ 0 & r_l & 0 \\ 0 & 0 & r_l \end{bmatrix} i_{abc} + \begin{bmatrix} l_l & 0 & 0 \\ 0 & l_l & 0 \\ 0 & 0 & l_l \end{bmatrix} \frac{d}{dt} i_{abc} \quad (10)$$

By using the following transforming equations, we obtain the following matricidal system:

Transformations from abc to $dq0$:

$$\begin{aligned} v_{zqd0} &= T(\Theta)v_{zabc} \\ v_{lqd0} &= T(\Theta)v_{labc} \\ i_{abc} &= T(\Theta)^{-1}i_{qd0} \end{aligned} \quad (11)$$

The system of equations ends up as follows:

$$v_{zqd0} - v_{lqd0} = T(\Theta) \begin{bmatrix} r_l & 0 & 0 \\ 0 & r_l & 0 \\ 0 & 0 & r_l \end{bmatrix} T(\Theta)^{-1}i_{qd0} + T(\Theta) \begin{bmatrix} l_l & 0 & 0 \\ 0 & l_l & 0 \\ 0 & 0 & l_l \end{bmatrix} \frac{d}{dt} (T(\Theta)^{-1}i_{qd0}) \quad (12)$$

Now, taking into account that for three-wire systems $i_0 = 0$, the voltage equations can be expressed as [8]:

$$\begin{bmatrix} v_{zq} \\ v_{zd} \end{bmatrix} - \begin{bmatrix} v_{zq} \\ v_{zd} \end{bmatrix} = \begin{bmatrix} r_l & l_l\omega_e \\ -l_l\omega_e & r_l \end{bmatrix} \begin{bmatrix} i_q \\ i_d \end{bmatrix} + \begin{bmatrix} l_l & 0 \\ 0 & l_l \end{bmatrix} \frac{d}{dt} \begin{bmatrix} i_q \\ i_d \end{bmatrix} \quad (13)$$

As we can see the $l_l\omega_e$ terms add the coupling relationship to the system. However, our main objective is to decouple them so that when voltages are applied in the q axis only current in the q axis is applied, with the exact same situation happening with the d axis.

By adding the following two variables we obtain an equation system in which the new q and d voltages depend only on the q and d currents respectively. Therefore, this substitution leads to a completely decoupled system. The last step is to apply Laplace

to take advantage of its properties and getting rid of the derivative. By doing so, i_q and i_d systems are obtained which only depend on the transfer function of the filter.

The new variables to decouple the system mentioned above are the following ones:

$$\hat{v}_{lq} = -v_{lq} + v_{zq} - l_l \omega_e i_d \quad (14)$$

$$\hat{v}_{ld} = -v_{ld} + l_l \omega_e i_q \quad (15)$$

The final equation system is as follows:

$$\begin{bmatrix} \hat{v}_{lq} \\ \hat{v}_{ld} \end{bmatrix} = \begin{bmatrix} r_l & 0 \\ 0 & r_l \end{bmatrix} \begin{bmatrix} i_q \\ i_d \end{bmatrix} + s \begin{bmatrix} l_l & 0 \\ 0 & l_l \end{bmatrix} \begin{bmatrix} i_q \\ i_d \end{bmatrix} \quad (16)$$

Now a suitable filter can be placed for each axis, which will have the main objective of cancelling out the dynamics imposed by the filter in order to impose our own dynamics. In the following figure a schematic model of a current control system is shown. As it can be seen, it contains both PI controllers as well as the decoupling loop.

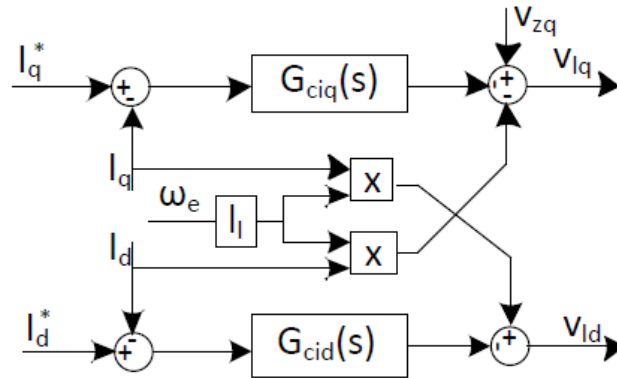


Figure 13: Representation of the current loop system [8].

Both controllers can be defined as:

$$G_{ciq}(s) = G_{cid}(s) = \frac{K_p s + K_i}{s} \quad (17)$$

Where both constants are expressed as [8]:

$$K_p = \frac{l_l}{\tau} \quad (18)$$

$$K_i = \frac{r_l}{\tau} \quad (19)$$

5.6.4. Current references computation

Since the DC side of the converter has been neglected, the current references are calculated in the following way:

$$P = \frac{3}{2} v_q i_q \quad (20)$$

$$Q = \frac{3}{2} v_q i_d \quad (21)$$

6. SIMULINK'S VSC MODEL

In this chapter the schematics and components used to model the voltage source converter explained in the previous chapter will be presented. Firstly, an overall view of the VSC set up will be shown.

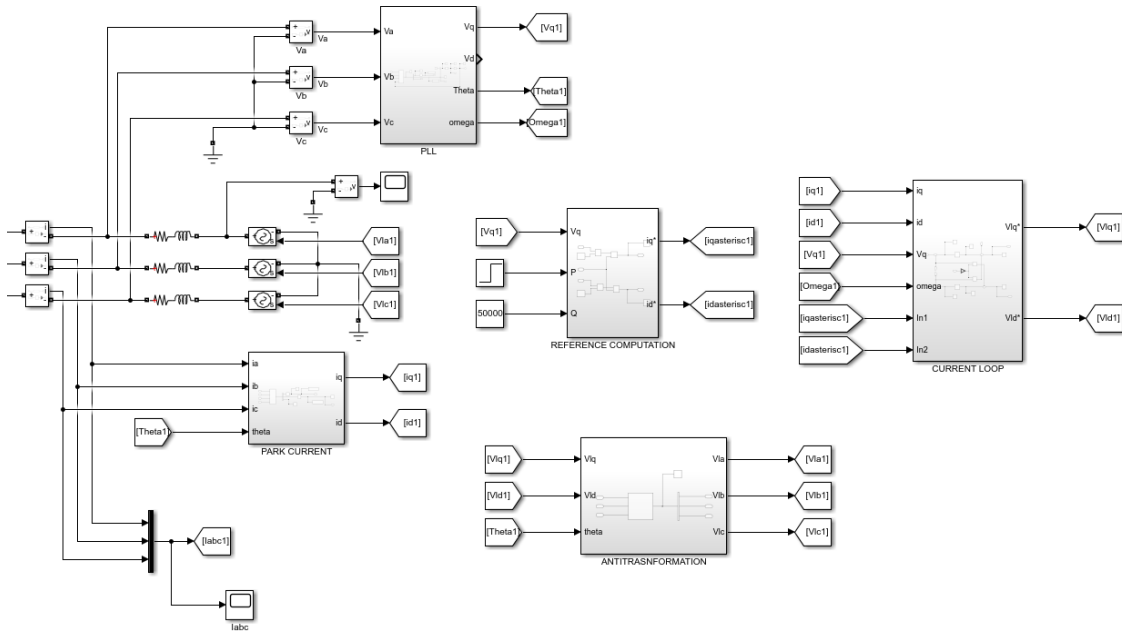


Figure 14: Overall view of one VSC converter and its control components in Simulink.

It is important to state that initially the grid was modelled as three AC voltage sources (such as shown in Figure 8), each one of them with a peak phase to neutral value of $400 \cdot \frac{\sqrt{2}}{\sqrt{3}}$ and with a frequency of 50 Hz. However, as it will be later shown, each VSC's AC side will lead to transformer which, in its turn, will lead to the grid. However, it is intended to maintain the low voltage side of the transformer at $400 \cdot \frac{\sqrt{2}}{\sqrt{3}}$.

6.1. Phase Locked Loop

As it can be seen from the image below, voltage measurements are taken from the grid's side.

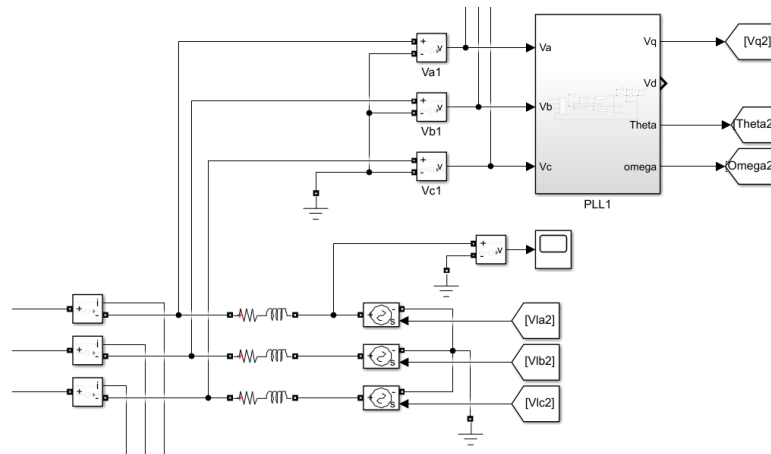


Figure 15: Display of VSC's AC side and the measurement of abc voltages.

These voltages are then transformed into $qd0$ quantities thanks to the closed loop explained before. As it can be seen in the figure below, the grid angle (Θ) is needed in order to apply the park transformation.

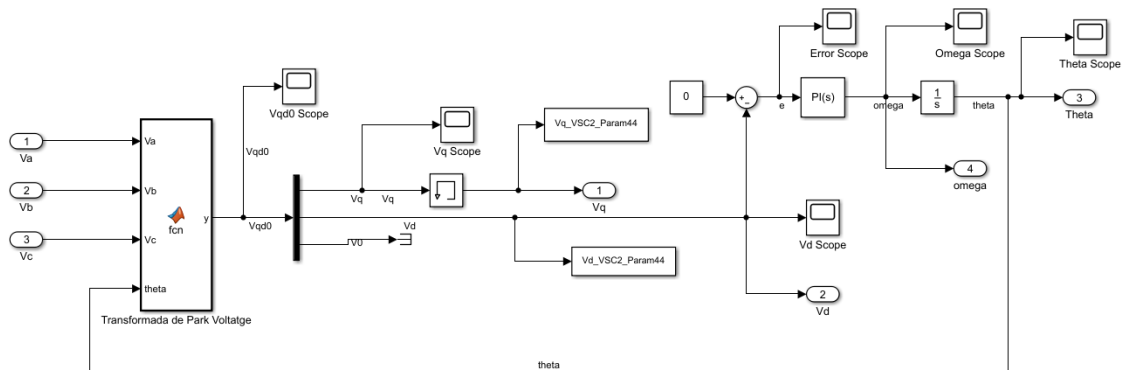


Figure 16: Phase Locked Loop in Simulink.

6.2. Reference computation

As stated in the previous chapter, when simplifying the system without adding the DC side of the converter, the current references are calculated with the Instantaneous Power Theory. The figure below shows the schematics of these calculations.

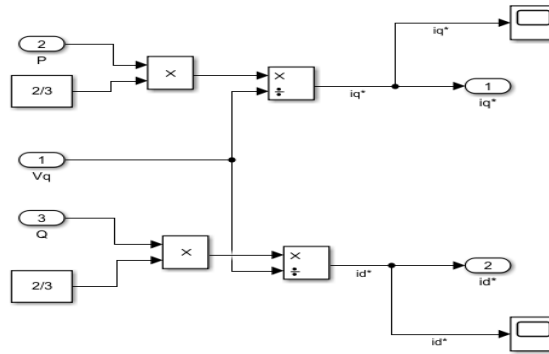


Figure 17: Current references computation in Simulink.

6.3. Current Control Loop

As for the current loop, the Park Transformation must be applied to the current passing through the filters. A key factor is to understand that the same grid angle obtained by the PLL is the one used for transforming the currents. Once these currents are calculated in the qd domain, they are compared with the current references as it can be seen below. Once the comparison has been made, the PI controllers eliminate the dynamics imposed by the filter in order to impose our own dynamics. Finally, the decoupling loop is added to effectively obtain independent control of both active and reactive power.

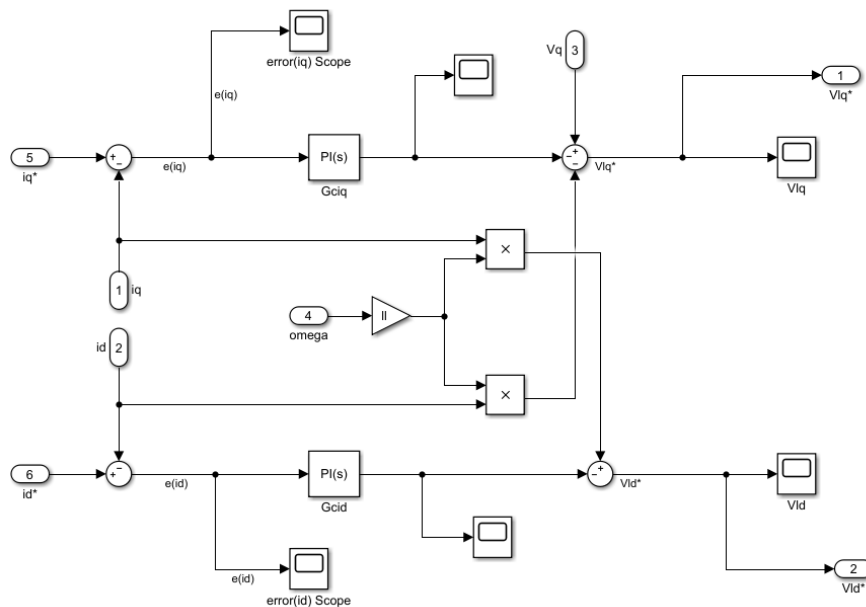


Figure 18: Current Loop in Simulink.

7. CABLES OF STUDY

The cable industry utilizes a wide variety of metallic conductors, but copper and aluminum are the most common ones. Above all characteristics and traits, conductivity, tensile resistance, weight and price are the most important ones.

Copper is, apart from silver, the most common metal conductor. Aside from its great conductivity, copper presents great tensile strength as well as good thermal conductivity.

Aluminum's history, on the other side, is not as old as copper's, but it has some properties which makes it extremely attractive. Although aluminum only has 60% of copper's conductivity, it weighs only 30% of its weight. As a result, an aluminum cable with the same electrical conductivity weighs only half of that one made of copper. Moreover, its price per unit is much cheaper, one third to be precise.

Now a brief comparison of their characteristics will be made:

Characteristics	Copper	Aluminum
Tensile Strength (lb/in ²)	50.000	32.000
Tensile Strength for same conductivity (lb/in ²)	50.000	50.000
Weight for same conductivity (lb)	100	54
Cross section for same conductivity.	100	156
Specific resistance (ohms-cir/mil ft) (20°C ref)	10.6	10.58
Coefficient of expansion (per deg. C x 10 ⁻⁶)	16.6	23

Table 2: Description of copper's and aluminum's main characteristics [9].

Copper is commonly used in the construction of small wires, where utilizing a small size does matter and therefore being able to take advantage of the copper's high electric conductivity is essential. For this reason, almost all electronic wires are made of copper. On the other hand, aluminum is now being used by cable companies in the construction of overhead lines, taking advantage of its low price and weight [10].

Due to the reasons stated above, aluminum is widely used for AC cables in solar power plants [11]. Although the cross section must be larger than that of copper to achieve the

same conductivity, the resultant tensile strength is the same and both its weight and price are reduced. Moreover, aluminum cable's lifetime is over 35 years. These last characteristics are of great importance as all big projects must find ways to reduce the total costs while maintaining optimum quality levels.

Once the material has been chosen, the cable values of Ohm/km, H/km and F/km were needed. Using the data sheet presented by Nexans and choosing a standard cross section of 300 mm², the following values were used:

	Values
Maximum AC Resistance	0,13 Ω /km
Inductance	$0,336 \cdot 10^{-3}$ H/km
Maximum Capacitance	$0,51 \cdot 10^{-6}$ F/km

Table 3: Impedance/km values [12].

8. SIMULATION

In this chapter a better description of the matter of study will be made. Moreover, the data report obtained through the simulations of each study case will be presented and discussed.

8.1. DESCRIPTION OF THE SYSTEM

As stated in the first chapter, this project studies the impact on the qd currents and voltages of the VSC converter when the system needs of longer medium voltage cables to connect each VSC to the grid.

The first step was to decide the global schematics and parameters of the system at hand. Therefore, it was determined that the solar park would consist of three different solar arrays, each one of them with its own VSC and with the ability of supplying 1 MVA. To help visualize the system of study, a schematic picture of the solar park and its connections to the grid will be presented.

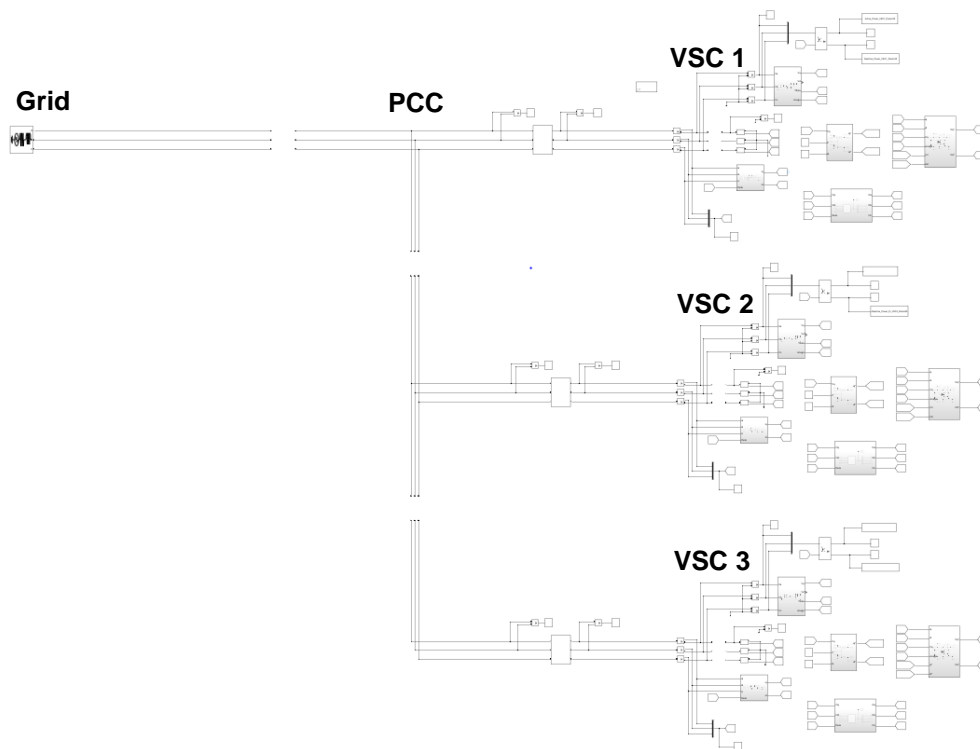


Figure 19: System under analysis comprising three VSC converters, three transformers, three medium voltage cables and the grid.

As it can be seen in the image above, each VSC's control system is modelled as described in the previous chapters, with its own PLL, current loop control, references

computation, etc. These components are modelled on the right-hand side of the image, one for each VSC.

All three converters are then connected to a transformer, which amplifies the voltage and therefore reduces the losses from Joule effect. The transformer's impedance values for a 1 MVA transformer are taken from the 'Short Circuit Fault Calculations' pdf mentioned in the bibliography [13].

Each transformer is then connected between medium voltage cables to the point of common coupling (PCC). Between the grid and the PCC there is a third medium voltage cable as it can be seen in the figure above.

As for the grid, it is modelled as a voltage source with its own source impedance and inductance. The 3-phase short-circuit level at base voltage (VA) is 100e6 and the X/R ratio is set to a value of 10.

The values used in the design of each VSC converter were taken from 'Active and Reactive power control grid connected distributed generation systems' pdf, also mentioned in the bibliography. However, it is important to state that both r_l and l_l values from the filters had to be sized in order to match the new power output. Therefore, the new values are:

$$r_l = 0.005 \Omega$$

$$l_l = 5,4 \cdot 10^{-5} \text{ H}$$

As stated before, because the DC side of the converter was simplified, both active and reactive power had to be set to a given value. To be precise, the power references used during the whole study are the following ones:

Time instant [s]	Active Power [KW]	Reactive Power [KVAr]
0	-300	-50
0.5	-500	-100

Table 4: Power inputs.

8.2. DESCRIPTION OF THE PARAMETRIC SIMULATIONS

Because the objective of this project is to vary the distance of each pi section line and study the effects of these cable length's variations on the qd currents, a parametric modeling must be performed. Therefore, an appropriate set of distances had to be chosen.

The average PV power plant with a capacity of 1 MW needs between 5000 and 6000 m² of land in order to get enough solar irradiance [14]. Assuming the estimated area results in 6000 m², a very plausible PV array configuration would be a portion of land of 200 m by 30 m covered with PV panels. Therefore, 0,5 km of pi section line would be considered a correct starting value for the simulations.

The other cable distances are presented below:

Simulation	Cable length [km]
1	0.5
2	1
3	2
4	5
5	10

Table 5: Display of distances studied.

To appropriately perform a correct analysis of the qd currents after every single cable distance variation, and to consider all possible situations, the following parametric studies were performed:

Simulation	Parametric	Cable 1 [km]	Cable 2 [km]	Cable 3 [km]
1	Param. 11	0,5	0,5	0,5
	Param. 12	1	0,5	0,5
	Param. 13	2	0,5	0,5
	Param. 14	5	0,5	0,5
	Param. 15	10	0,5	0,5
2	Param. 21	0,5	0,5	0,5

	Param. 22	0,5	1	0,5
	Param. 23	0,5	2	0,5
	Param. 24	0,5	5	0,5
	Param. 25	0,5	10	0,5
3	Param. 31	0,5	0,5	0,5
	Param. 32	0,5	0,5	1
	Param. 33	0,5	0,5	2
	Param. 34	0,5	0,5	5
	Param. 35	0,5	0,5	10

Table 6: Display of all cable length's configurations.

As it can be seen in the table above, the first parametric modeling involves the evaluation of pi section lines 1 while the other two sets of cables remain constant at 0,5 km. The parametric modeling 2 involves the study of pi section lines 2 while parametric modeling 3 involves pi section lines 3.

In order to understand which number is given to which cable, the following image is presented:

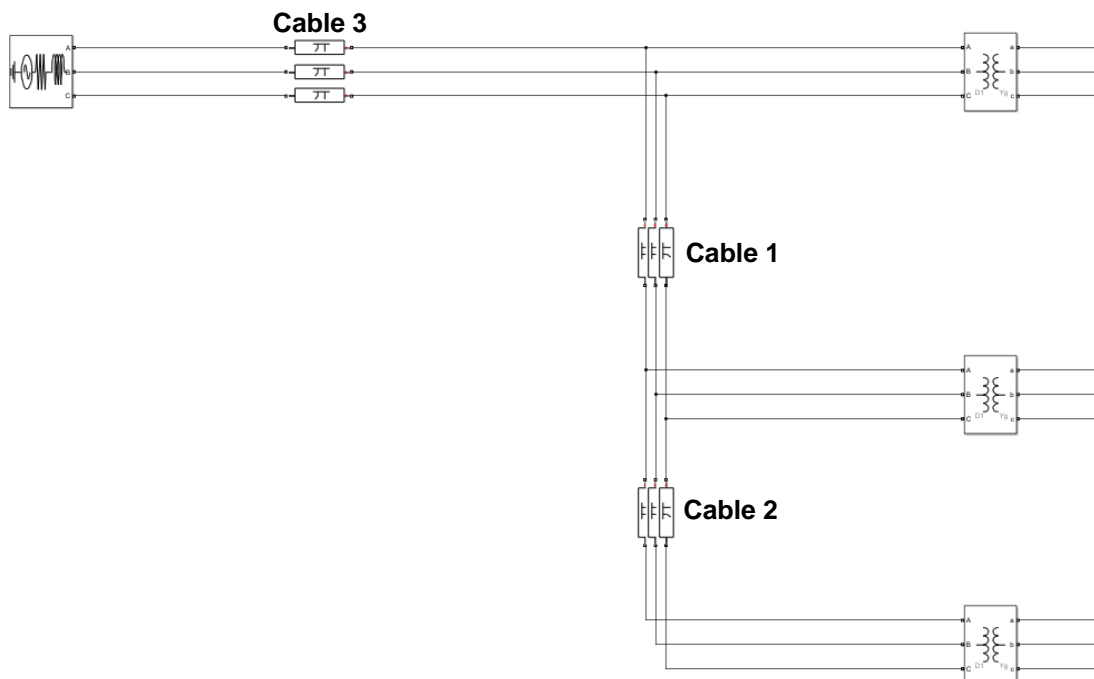


Figure 20: Identification of the cables of study.

It is important to state that each simulation is run for 1 second. Moreover, as stated before, the objects of study are the currents and voltages in the qd domain. Current is the magnitude which historically causes more difficulties for converters to control. Hence, it will be looked at first.

8.3. CABLE'S MODEL SELECTION

Once the material of choice (aluminum) and its impedance values per kilometer are established, the cable model must be chosen. Simulink offers a few models in order to simulate cable lines. In this project, before making any final decision, two different models were studied:

- RL series branch.
- Pi section line.

The latter considers the capacitive effect of real-life cables lines. This effect involves the conductors of the transmission line, which act as a capacitor plate with the air being the dielectric medium between them. On the other hand, RL series branches are a simplification of the mentioned Pi section lines.

To appropriately perform a comparison between these two models, a simulation where the VSC parameters would be highly tested was carried out. Therefore, after carrying out a series of simulations, it was analyzed that cable 3 (go to Figure 22 for better understanding) had the biggest impact on all three VSC's variables. Consequently, this cable's length was increased to 10 km while leaving the other cable's lengths at the base value of 0,5 km.

Finally, a complete simulation was carried out with both cables. In the first simulation all cables were modelled with RL series branches and in the latter simulation they were modelled with Pi section lines.

The data obtained from q and d currents at VSC1 through the comparison is shown below:

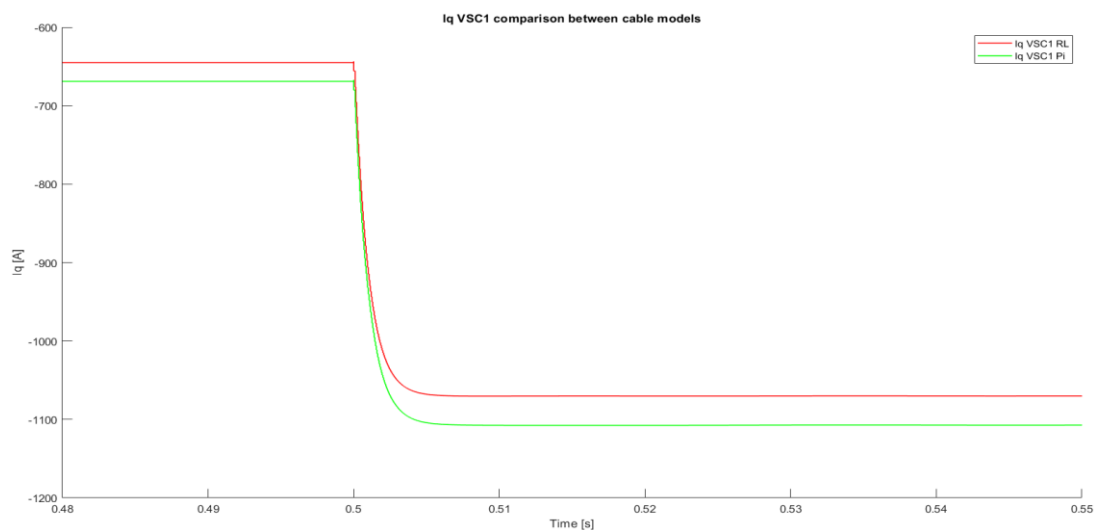


Figure 21: VSC1's i_q magnitude comparison when using RL series branches and Pi section line.

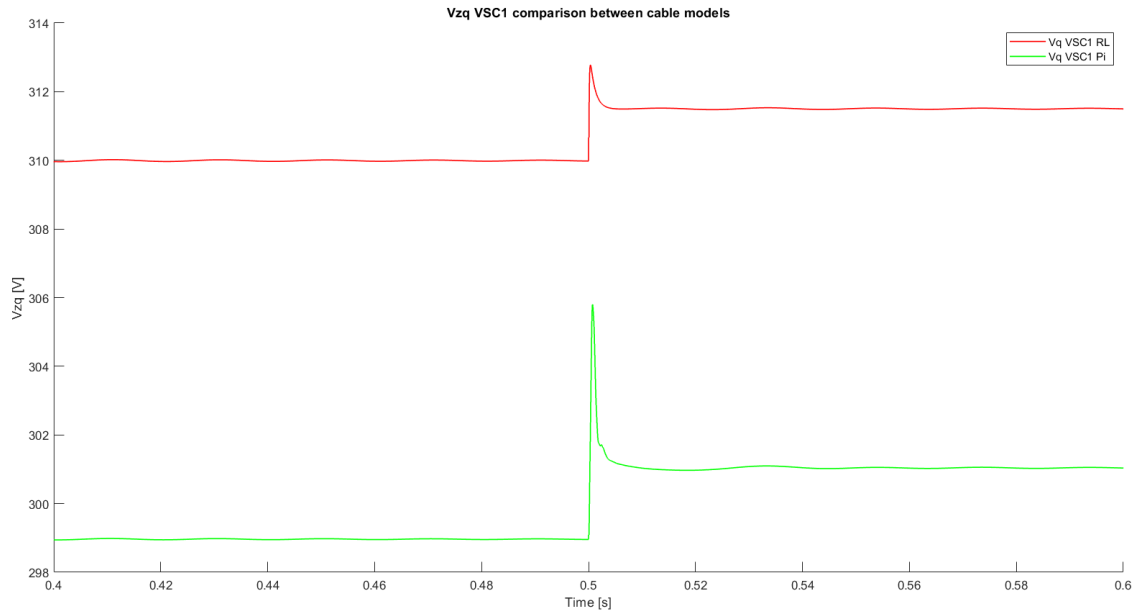


Figure 22: VSC1's V_{zq} from the LV side of the transformer magnitude comparison when using RL series branches and Pi section line.

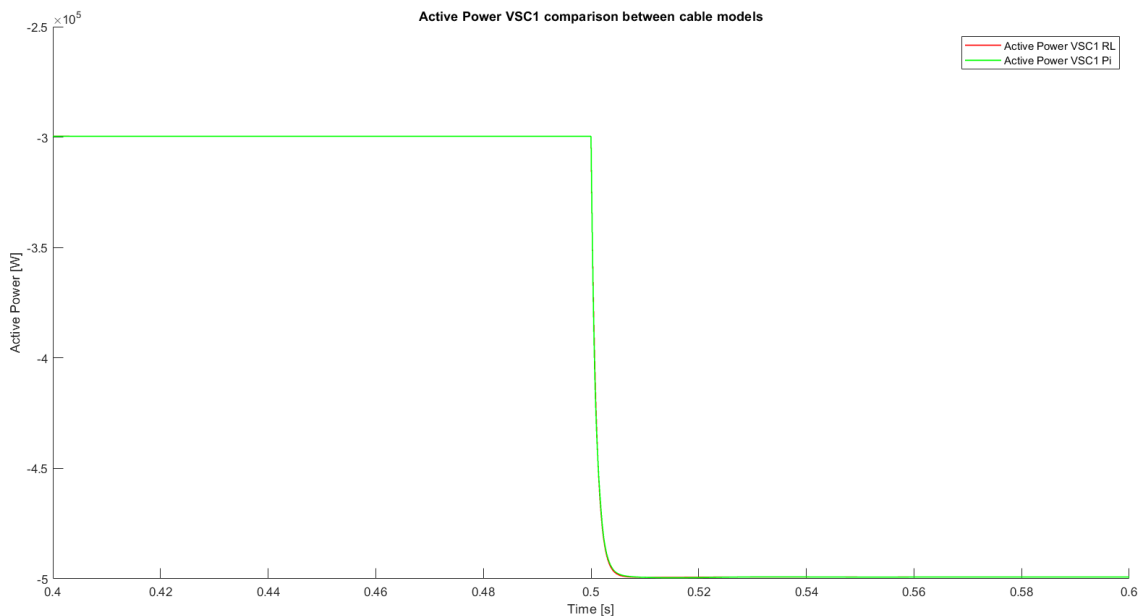


Figure 23: VSC1's Active Power magnitude comparison when using RL series branches and Pi section line.

Data obtained from the remaining two converters was deemed unnecessary because it showed similar results to those obtained from VSC1.

In conclusion, although with both cable models the converter is supplying to the grid the intended active power (see Table 4), both q magnitudes (current and voltage) show a significant difference. Therefore, in order to perform a more realistic study the medium voltage cables were represented with the pi section lines that Simulink offers.

8.4. SIMULATION 1

As stated before, in this simulation cable's 1 impedance values per kilometer will be increased until reaching a threshold value of 10 km.

It is important to state that the initialization of the system involves sudden spikes of the variables at hand. Their values shall not be taken into consideration nor studied because they don't represent reality. Therefore, this project will focus on the behavior of the system when going from one steady state to another. This is achieved by changing either the active or reactive power inputs as shown in the previous chapter (at 0,5 seconds).

Firstly, q currents data will be presented:

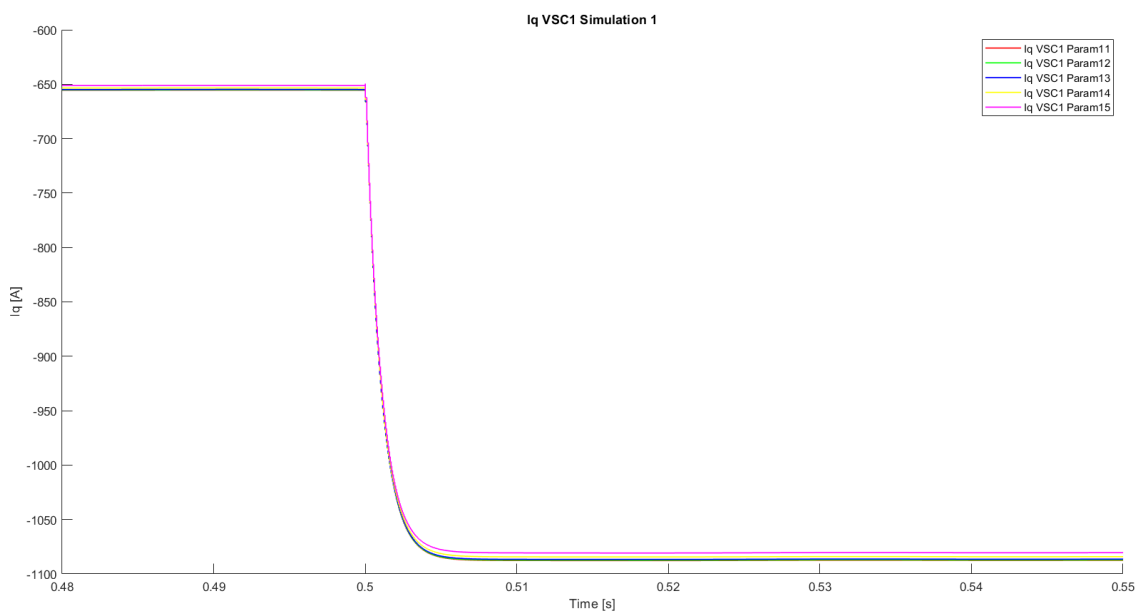


Figure 24: VSC1's i_q magnitude comparison during simulation 1.

Since the reference computation magnitude i_q^* is calculated by isolating set magnitude from equation 20, when varying the cable length, V_{zq} also varies. Therefore, the circuit currents changes as it can be seen in Figure 23.

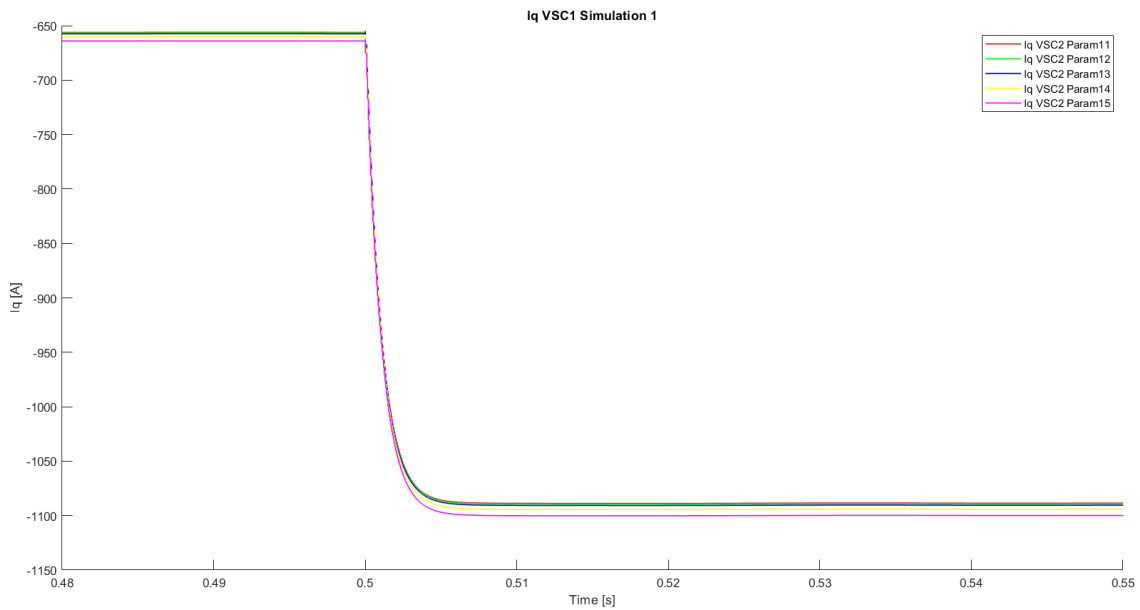


Figure 25: VSC2's i_q magnitude comparison during simulation 1.

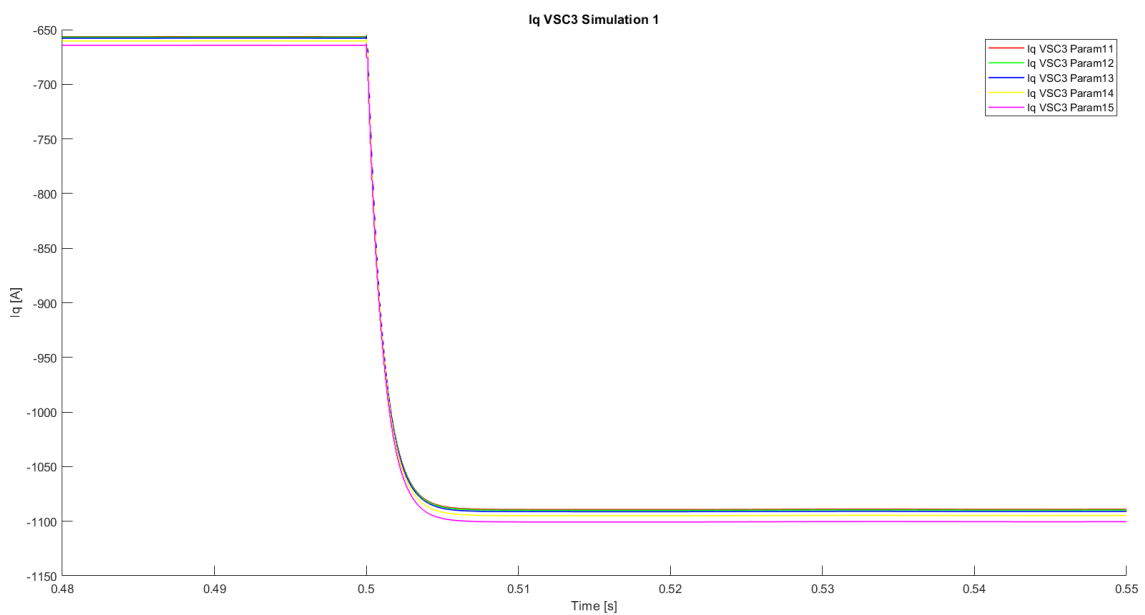


Figure 26: VSC3's i_q magnitude comparison during simulation 1.

Regarding VSC's 2 and 3, the tendency obtained is the opposite. As it will be shown in the following pages, V_{zq} from VSC one increases while V_{zq} from VSC two and three decreases. This effect is obtained because cable one is placed between both converters and the point of common coupling (PCC).

Now d current data will be presented:

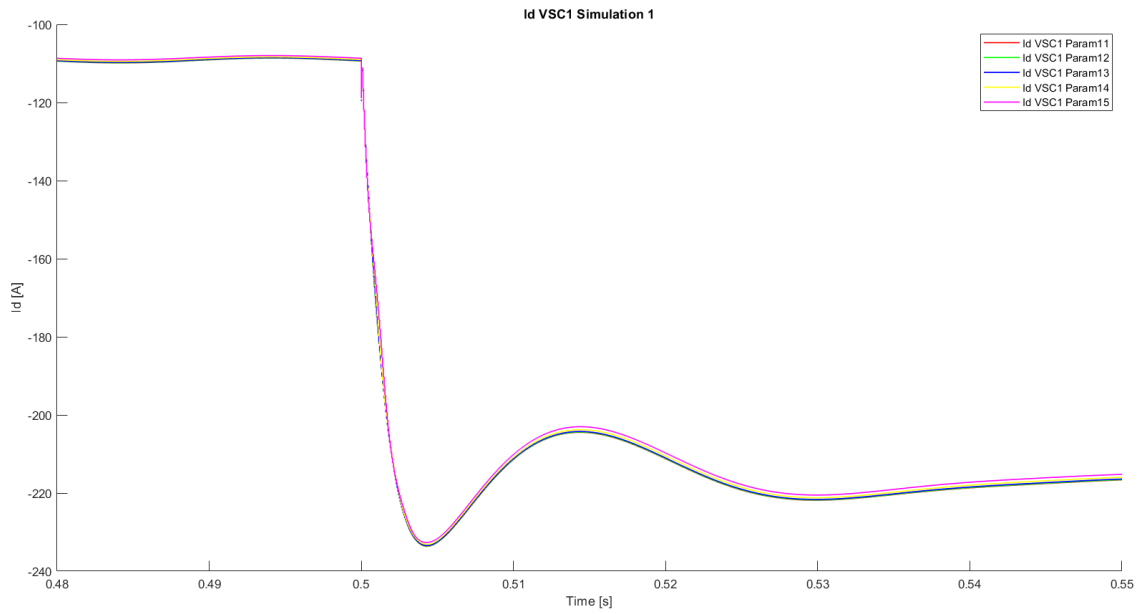


Figure 27: VSC1's i_d magnitude comparison during simulation 1.

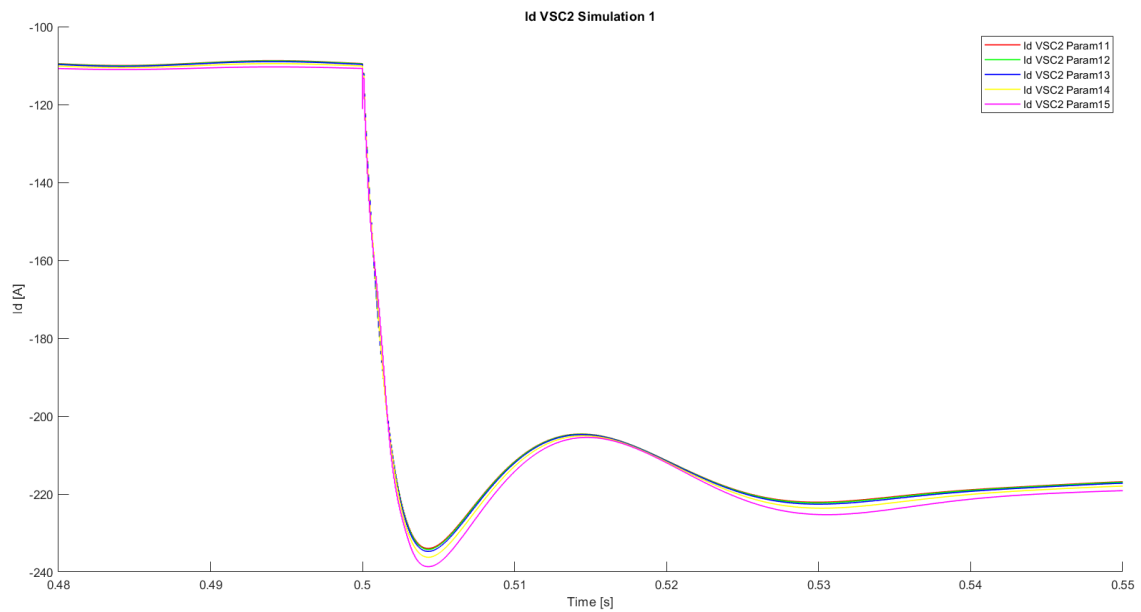


Figure 28: VSC2's i_d magnitude comparison during simulation 1.

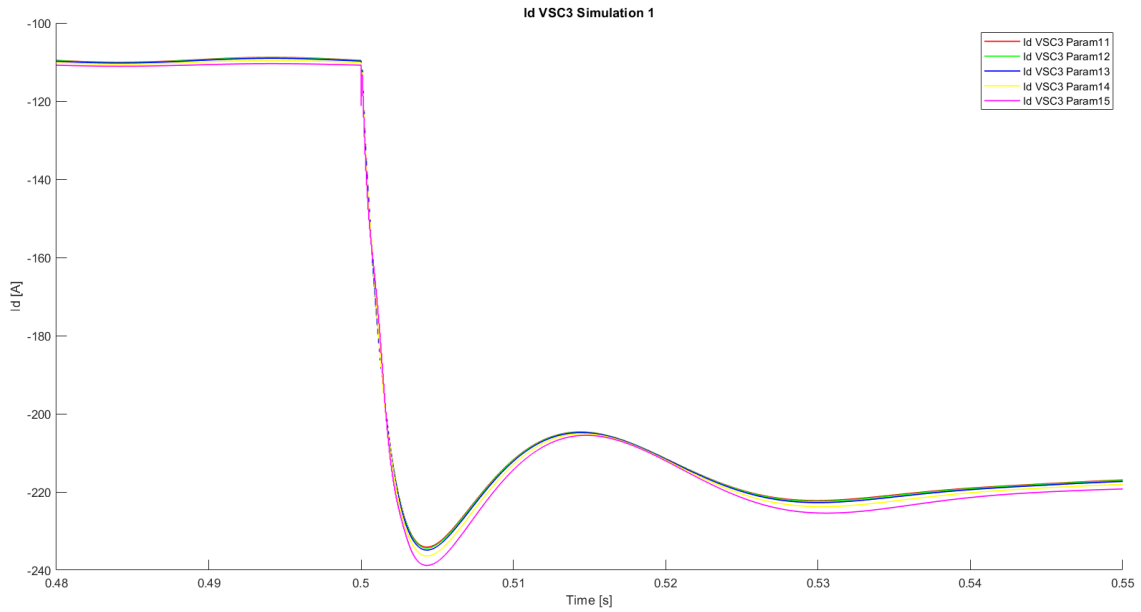


Figure 29: VSC3's i_d magnitude comparison during simulation 1.

Instead of a first order response when transitioning from one steady state to another, i_d currents transition following a second order response as it can be seen from the Figures above.

For a better understanding of the evolution of q current magnitudes (related to active power), V_{zq} magnitudes will be shown:

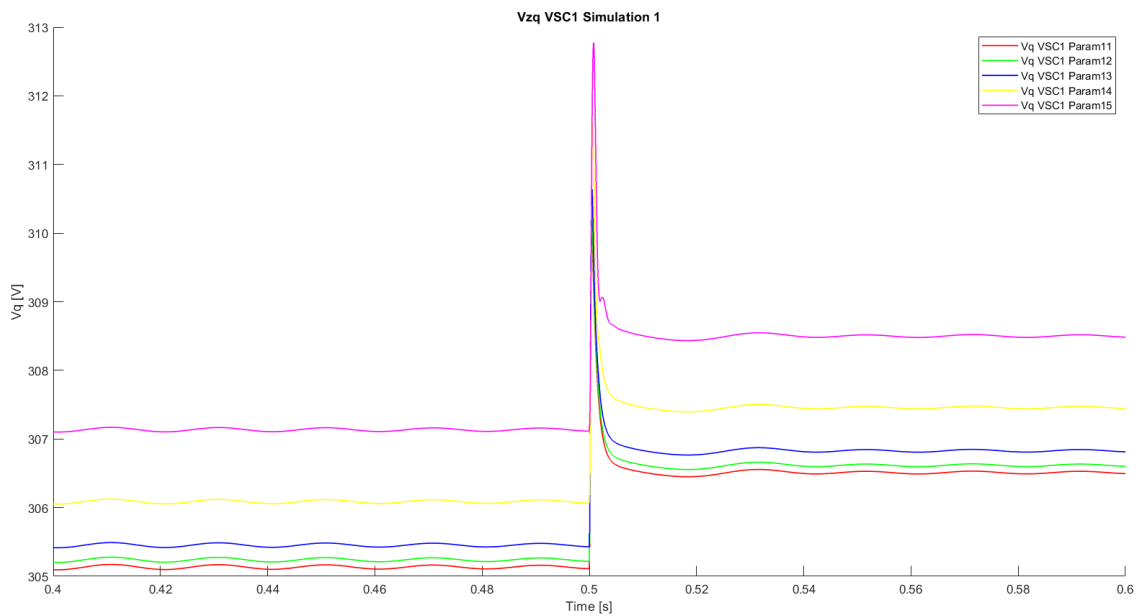


Figure 30: VSC1's V_{zq} magnitude comparison during simulation 1.

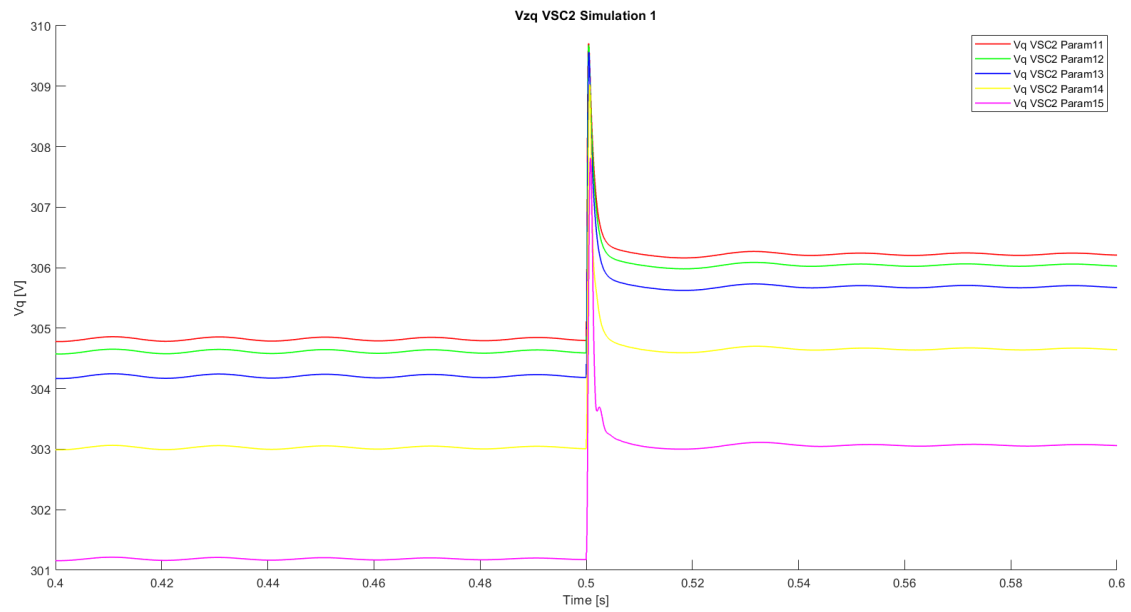


Figure 31: VSC2's V_{zq} magnitude comparison during simulation 1.

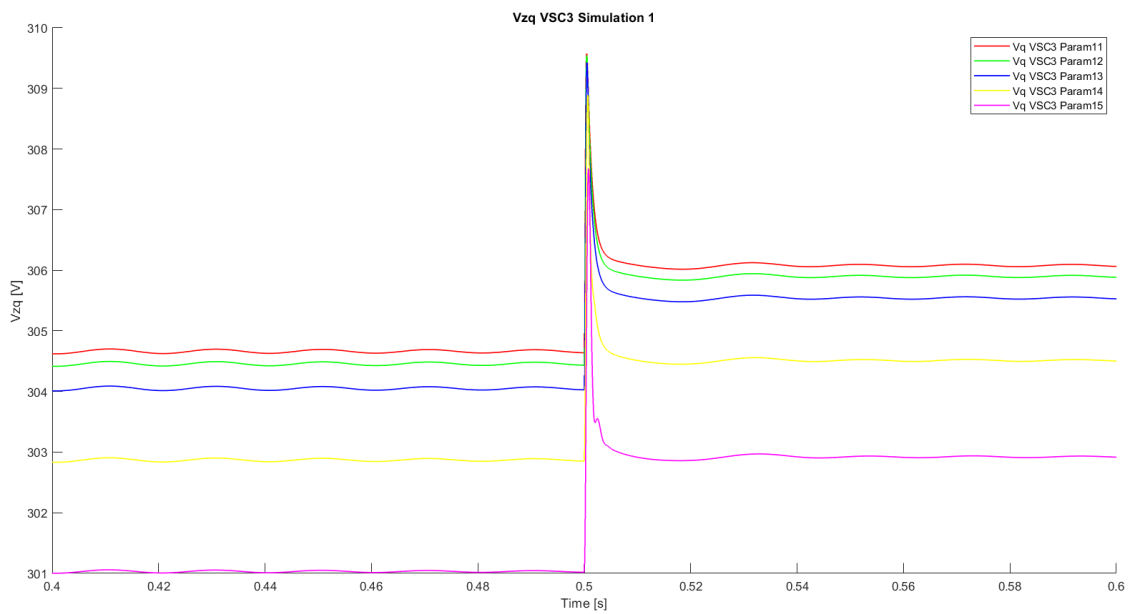


Figure 32: VSC3's V_{zq} magnitude comparison during simulation 1.

As it can be seen from Figure 30, VSC1's voltage measurement before reaching the transformer experiences an increase in magnitude proportionally to the increase of cable line one. Hence, the decrease in current.

As for q currents from VSC two and three, their system's V_{zq} has an inversely proportional relationship with the increase of the cable line. Hence, the increase in their q current magnitudes.

Finally, the active power response for all three converters will be shown.

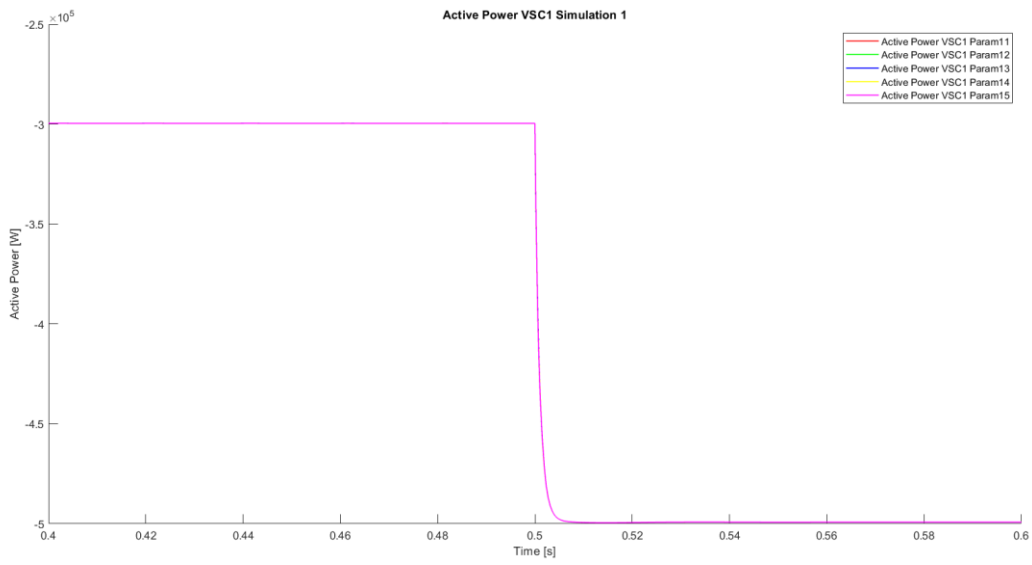


Figure 33: VSC1's active power magnitude comparison during simulation 1.

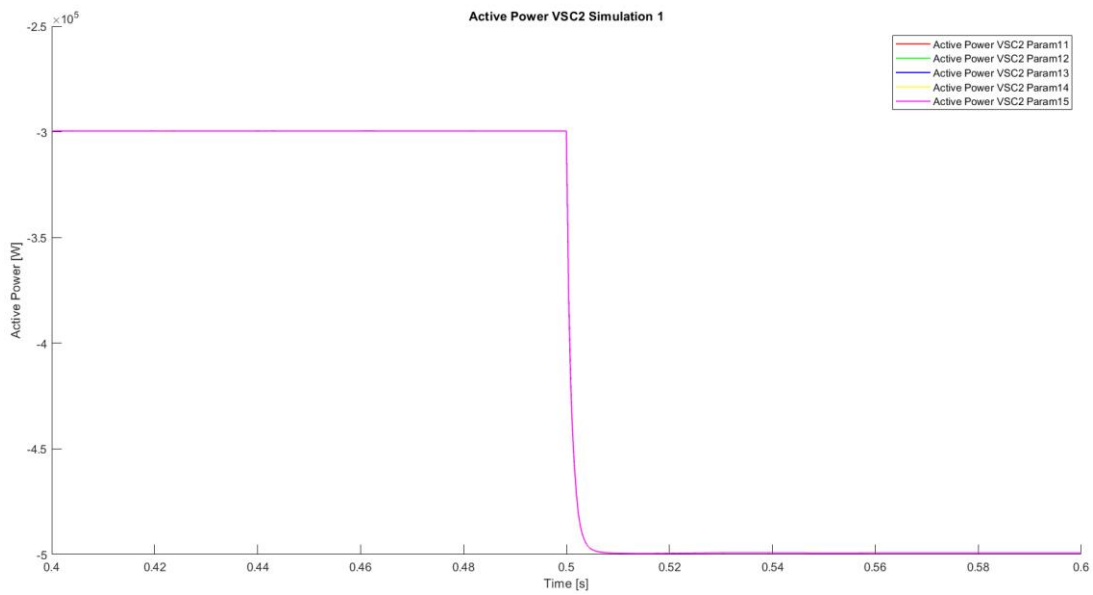


Figure 34: VSC2's active power magnitude comparison during simulation 1.

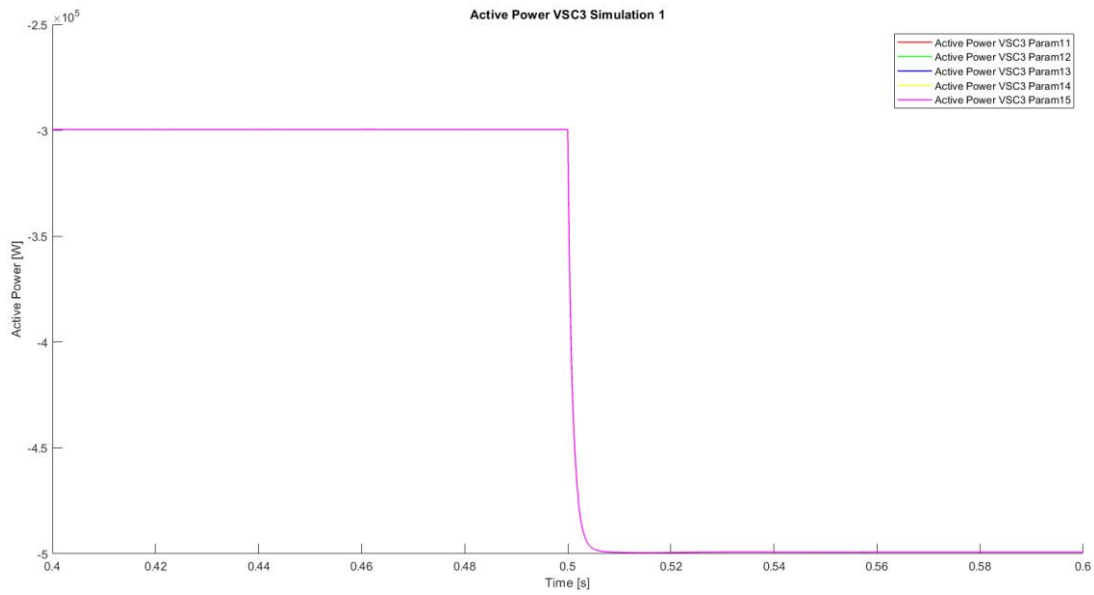


Figure 35: VSC3's active power magnitude comparison during simulation 1.

As it can be seen from the Figures above, the active power supplied by the voltage source converters remains unaltered by the variation of cable length. In other words, both steady state magnitudes correspond to the active power reference inputs. However, as it can be seen, the transition is not immediate and its accomplished with a first order response.

8.5. SIMULATION 2

As stated before, in this simulation cable's 2 impedance values per kilometer will be increased until reaching a threshold value of 10 km.

Following the course of action from simulation 1, only images from the transient state at 0,5 seconds will be shown.

Firstly, q currents will be shown:

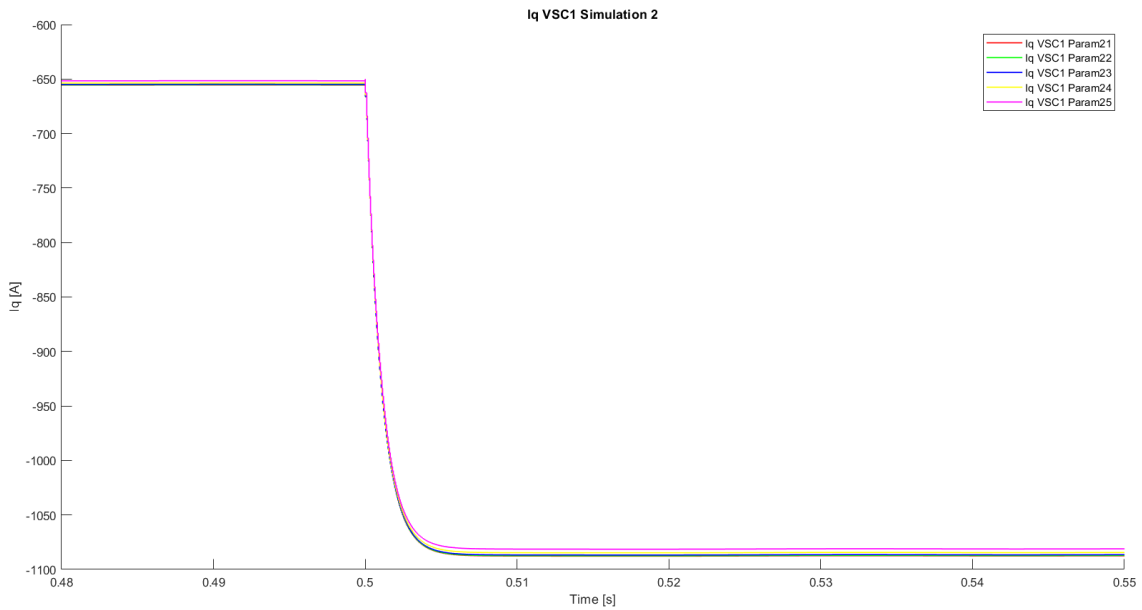


Figure 36: VSC1's i_q magnitude comparison during simulation 2.

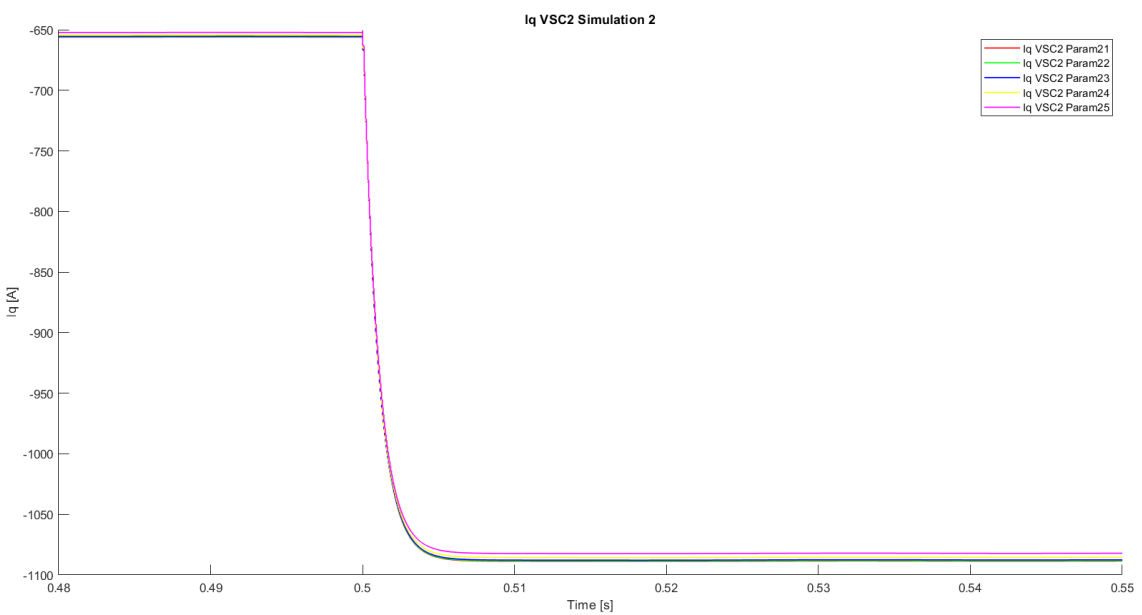


Figure 37: VSC2's i_q magnitude comparison during simulation 2.

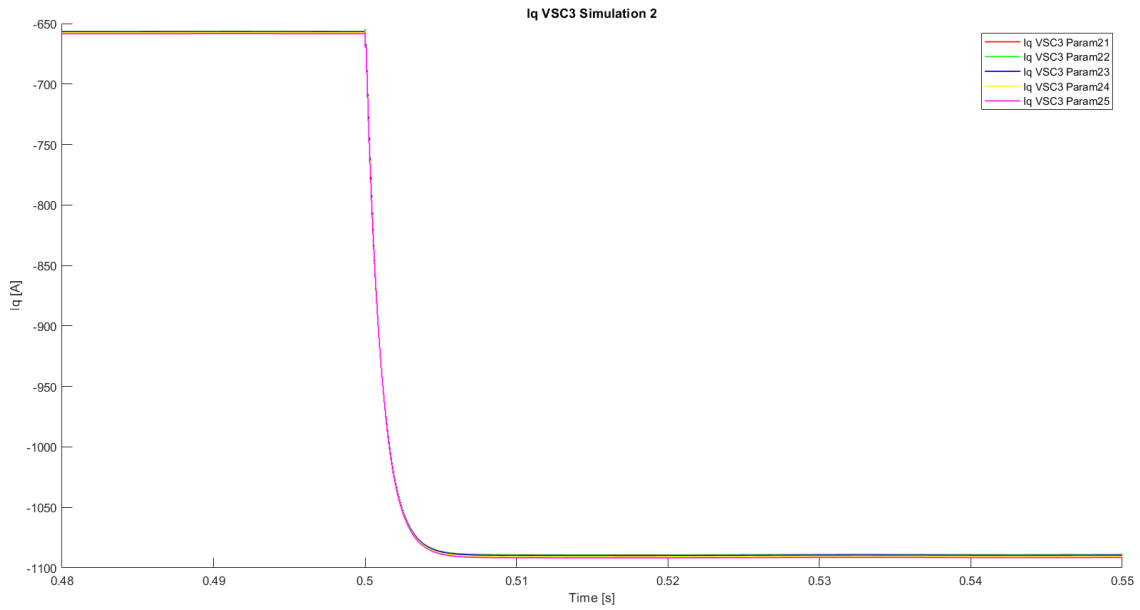


Figure 38: VSC3's i_q magnitude comparison during simulation 2.

As stated in the previous simulation, the current reference calculation is obtained from isolating i_q^* from equation 20. Consequently, V_{zq} magnitude varies which, as a result, makes q current magnitudes vary.

Due to the placement of the cable of study, VSC one and two obtain the same data. On the other hand, the third converter's data shows an opposite reaction. As the cable length is increased, so do the values of the q current. A key statement to underline is the fact that q current quantities seem to be less sensible to varying cable's two length compared to cable one.

Secondly, d currents will be presented:

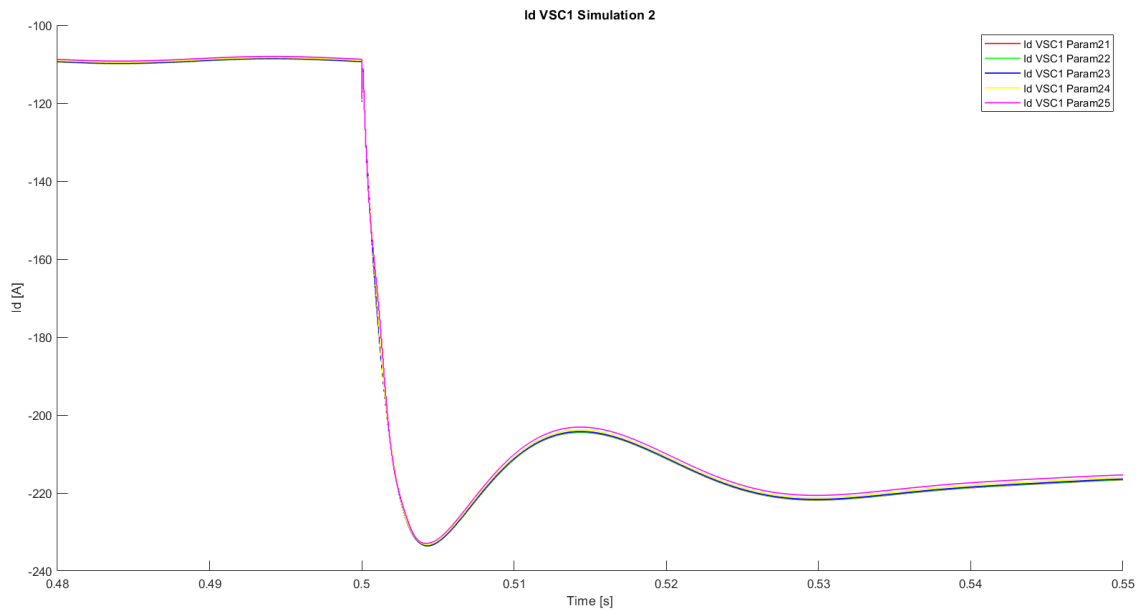


Figure 39: VSC1's i_d magnitude comparison during simulation 2.

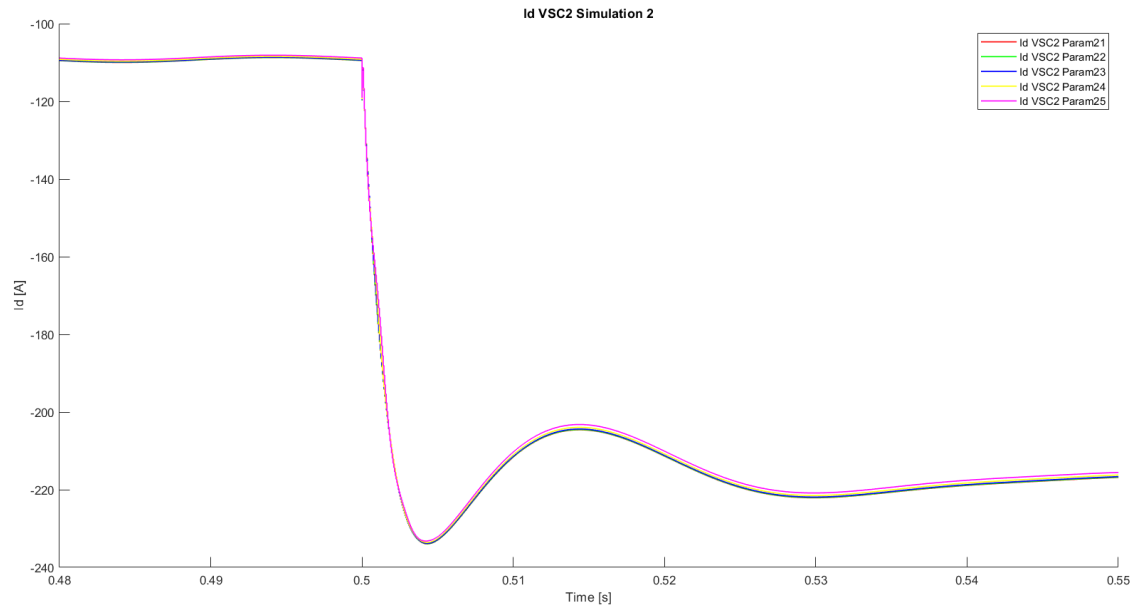


Figure 40: VSC2's i_d magnitude comparison during simulation 2.

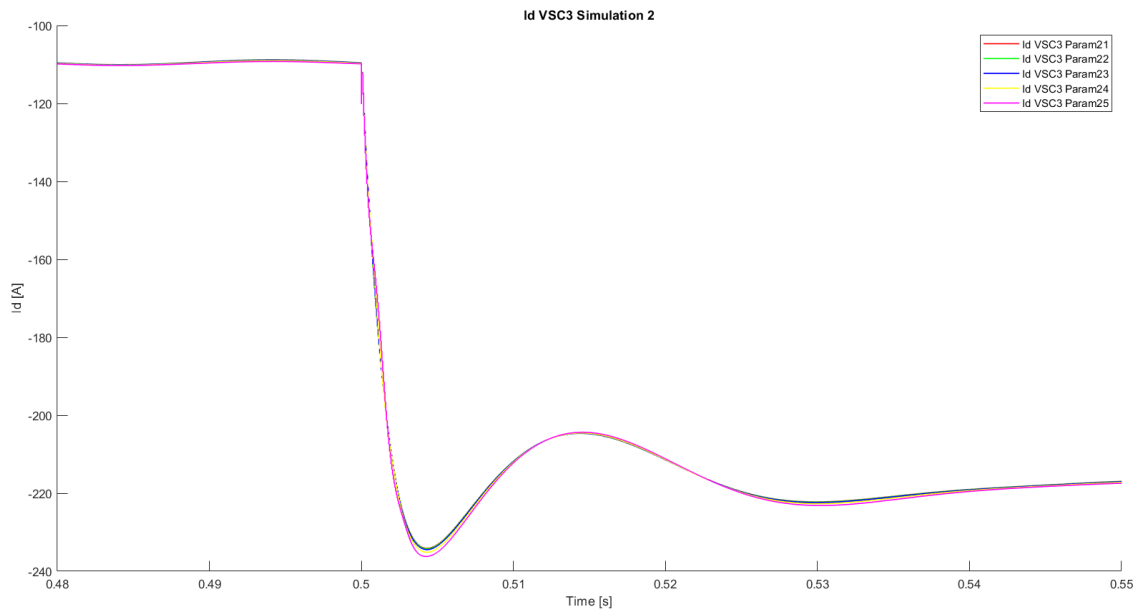


Figure 41: VSC3's i_d magnitude comparison during simulation 2.

Mirroring the behavior from the previous simulation, d currents from the converters present a brief oscillatory reaction at 0,5 seconds. Moreover, the overshoot values for the converters placed below (VSC 3) the cable of study display higher peak values as the distance increases, whereas the converters placed above the pi section line of study display very little difference between simulations.

Regarding V_{zq} data for each converter, it is shown below:

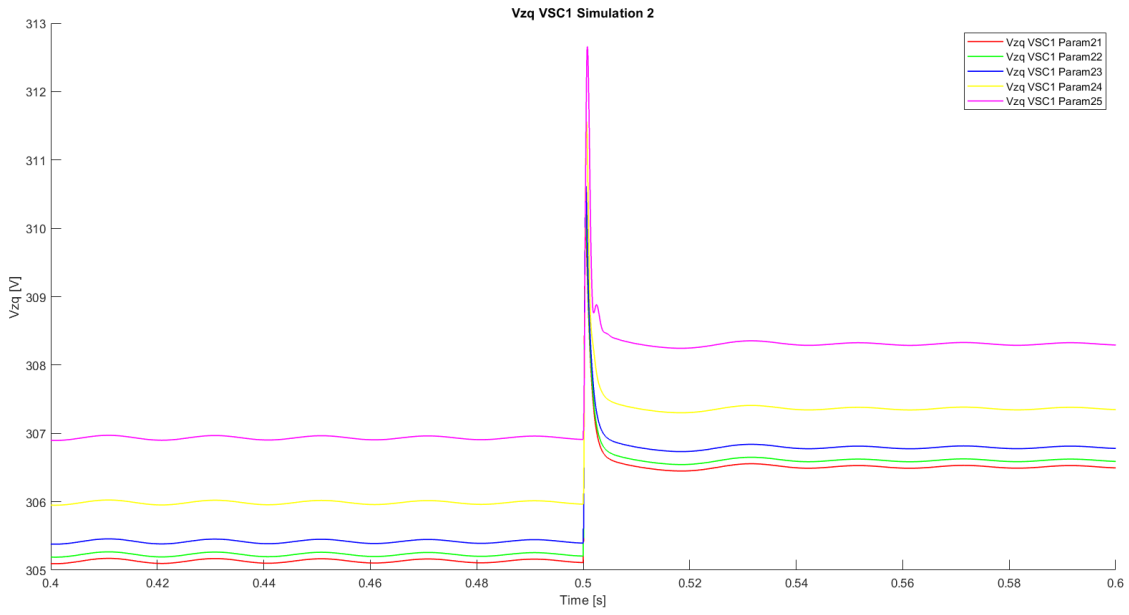


Figure 42: VSC1's V_{zq} magnitude comparison during simulation 2.

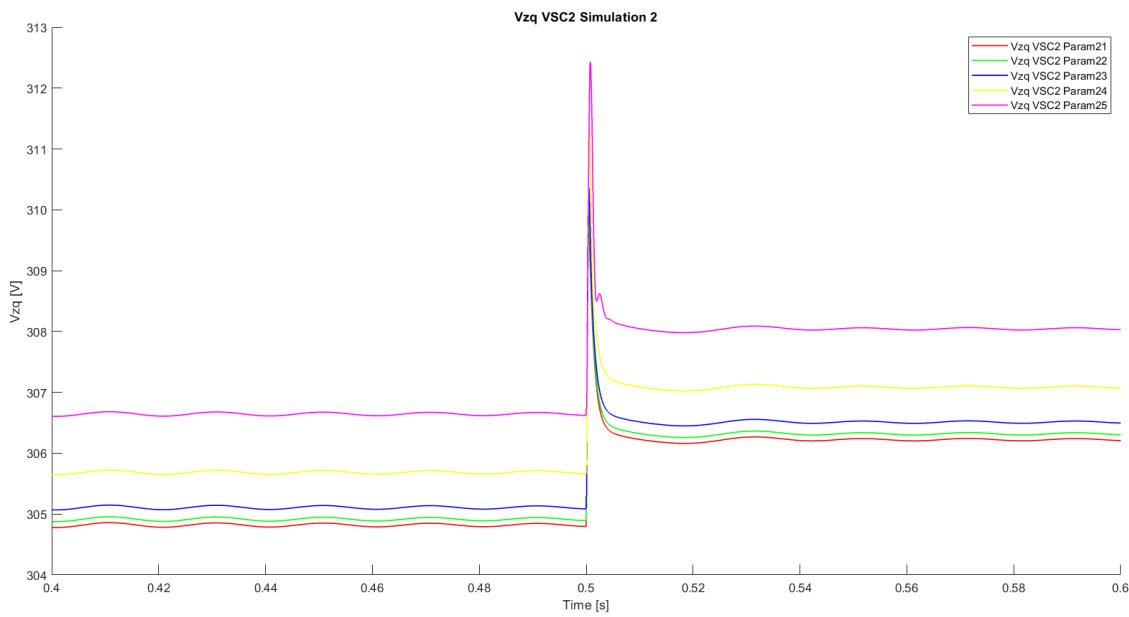


Figure 43: VSC2's V_{zq} magnitude comparison during simulation 2.

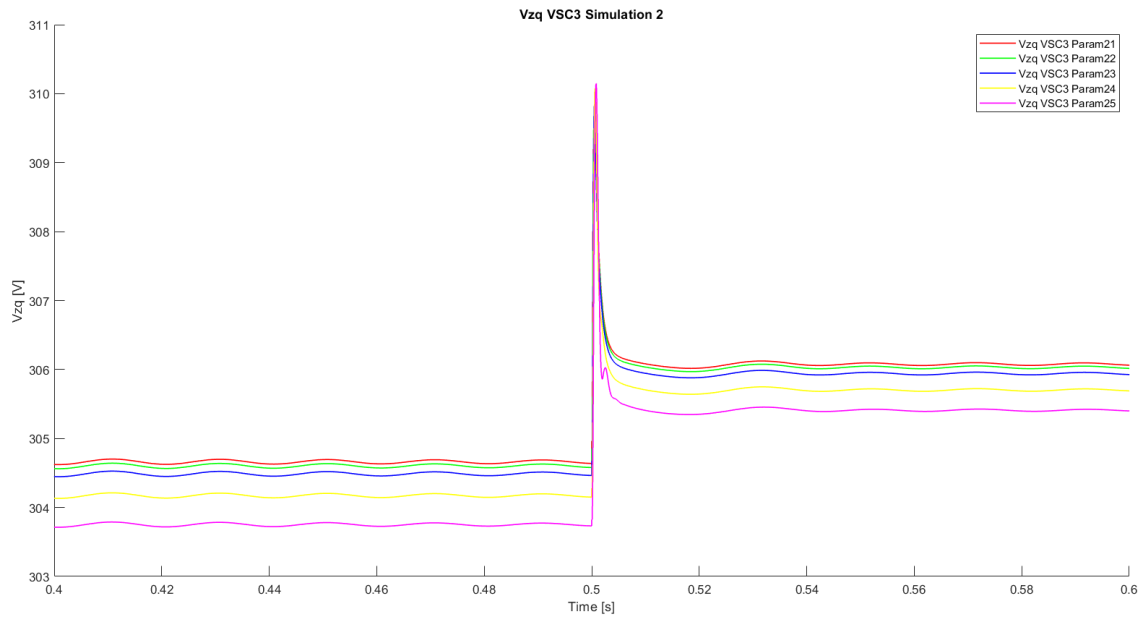


Figure 44: VSC3's V_{zq} magnitude comparison during simulation 2.

As it can be seen from Figure 42 to 43, VSC1's and 2 voltage measurement before reaching the transformer experiences an increase in magnitude proportionally to the increase of cable line one. Hence, the decrease in current.

As for q currents from VSC three, its system's V_{zq} has an inversely proportional relationship with the increase of the cable line. Hence, the increase in their q current magnitudes.

Finally, active power data will be displayed:

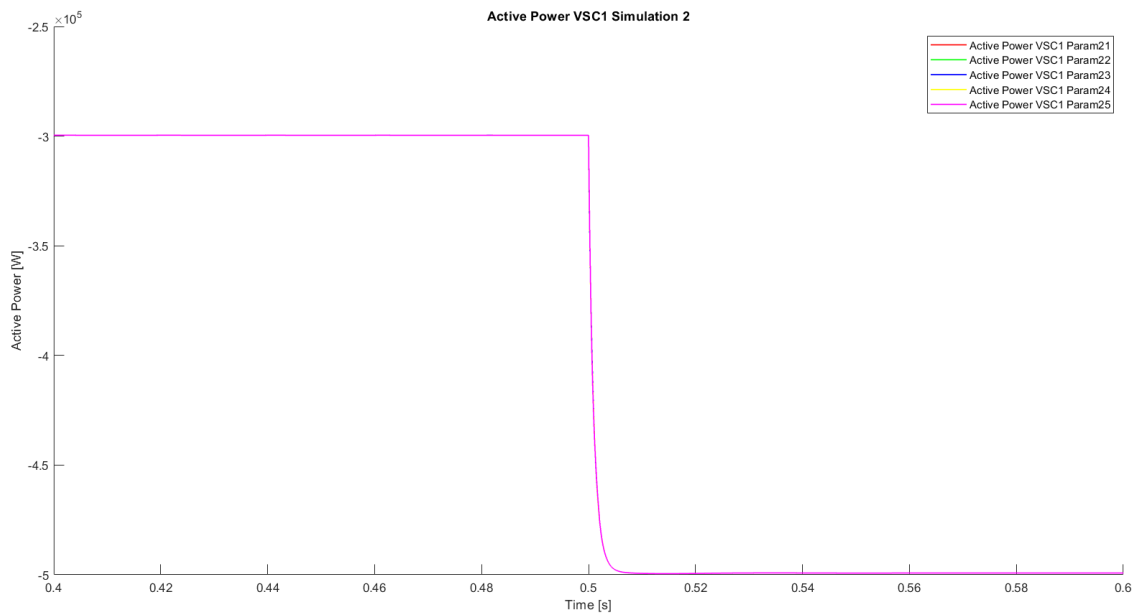


Figure 45: VSC1's active power magnitude comparison during simulation 2.

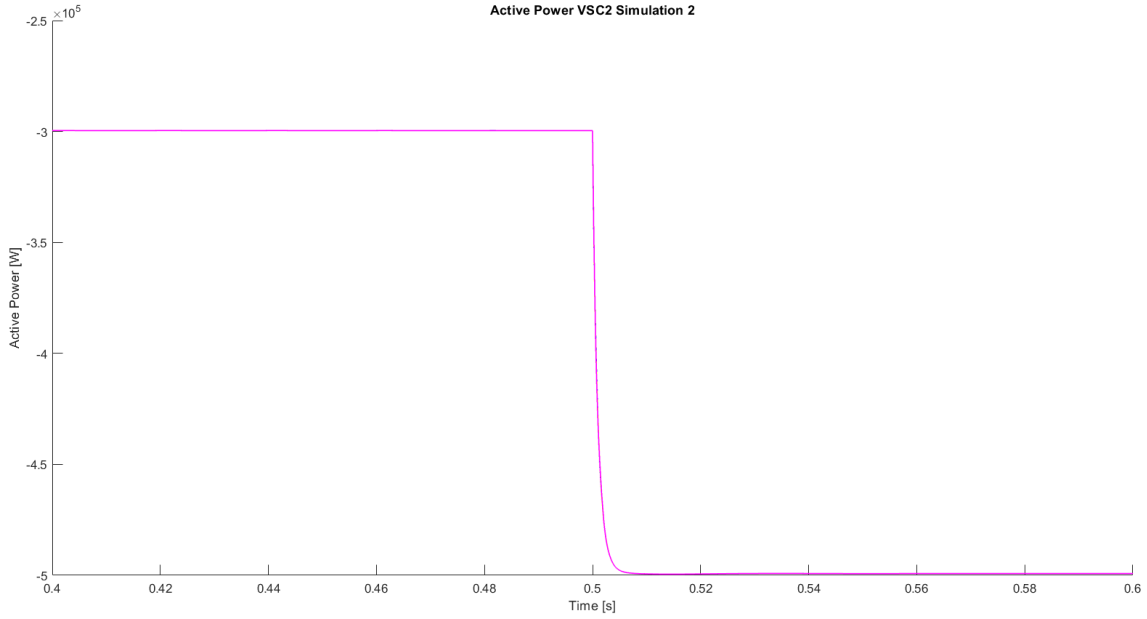


Figure 46: VSC2's active power magnitude comparison during simulation 2.

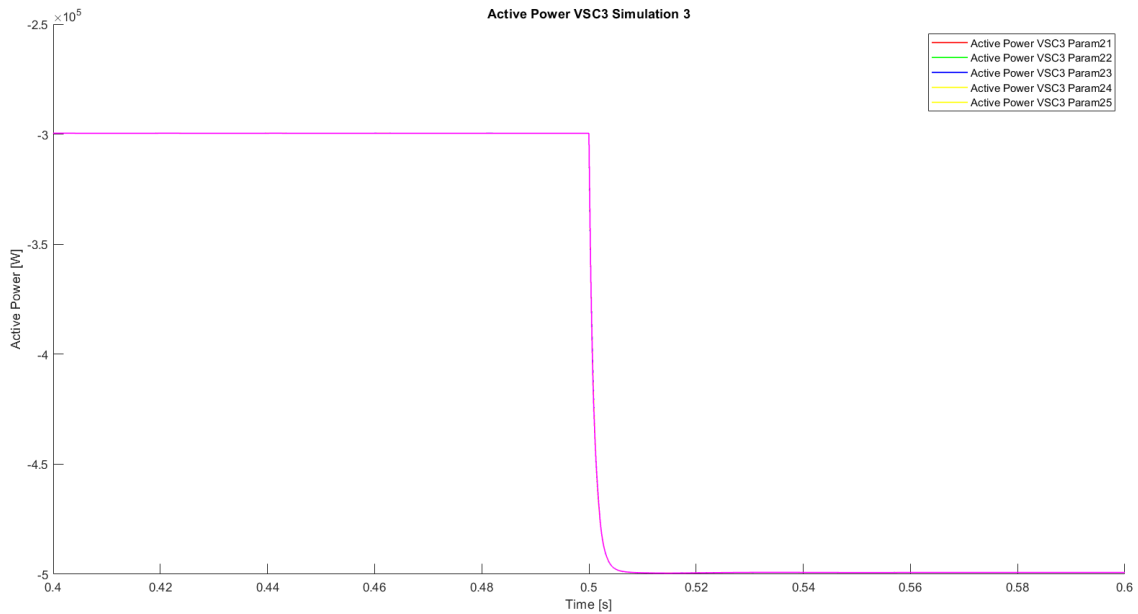


Figure 47: VSC3's active power magnitude comparison during simulation 2.

As it can be concluded from the overlapping of all the data above, the active power supplied by all three converters remains unaltered when varying cable's two length. The transition from one steady state to another mirrors the behavior obtained from simulation one.

8.6. SIMULATION 3

As stated before, in this simulation cable's 3 impedance values per kilometer will be increased until reaching a threshold value of 10 km. An important factor to keep in mind is that for this simulation the cable of study is situated between the point of common coupling and the grid.

Following the course of action from simulation 1, only images from the transient state at 0,5 seconds will be shown.

The q current's transient state simulations are shown below:

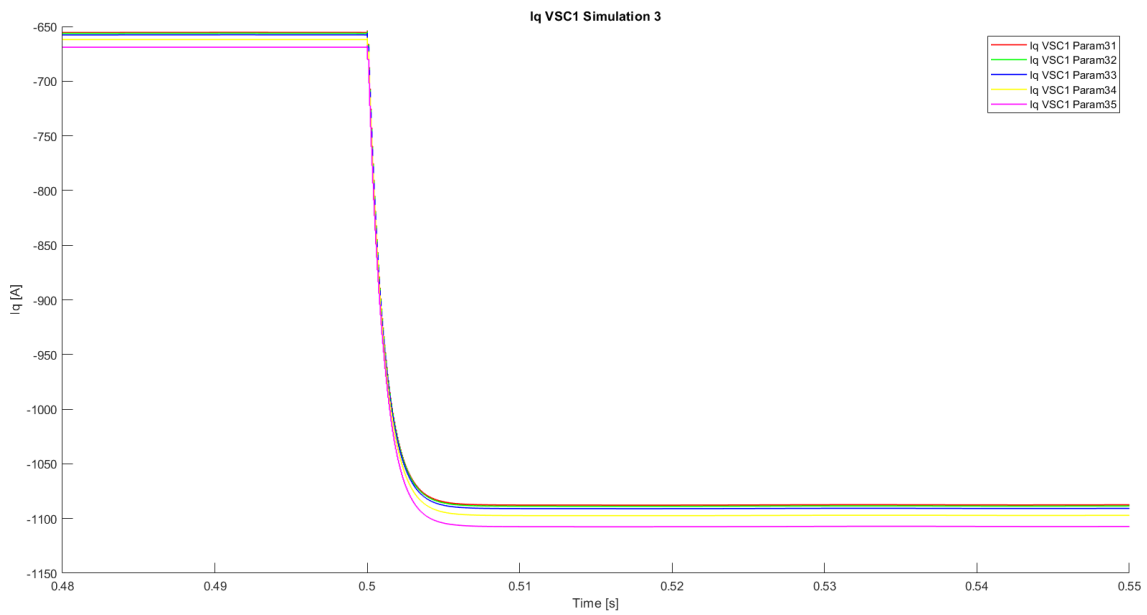


Figure 48: VSC1's i_q magnitude comparison during simulation 3.

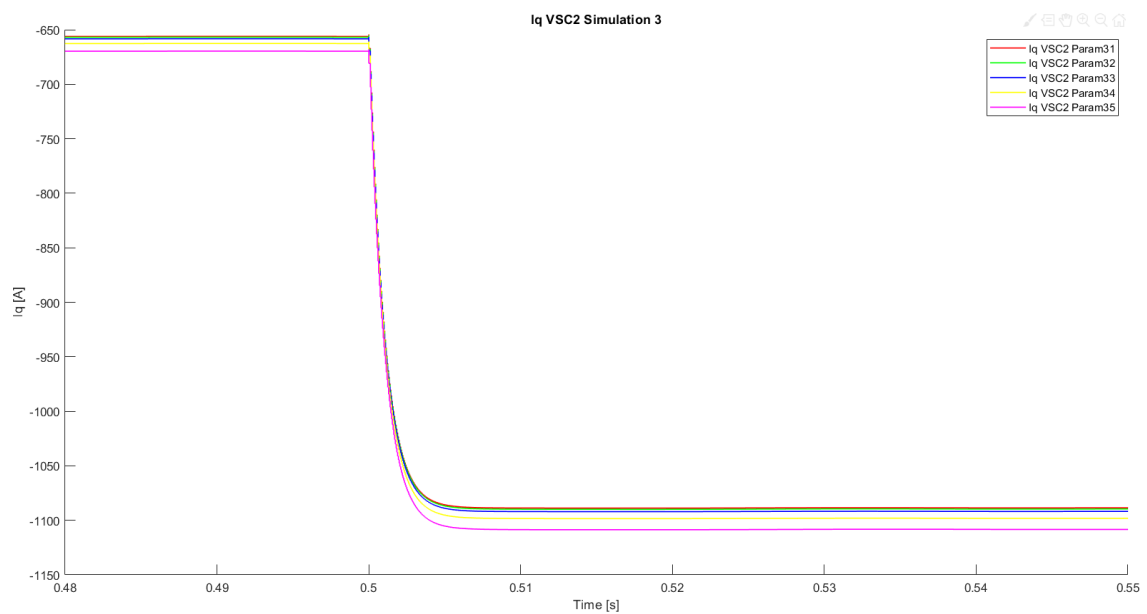


Figure 49: VSC2's i_q magnitude comparison during simulation 3.

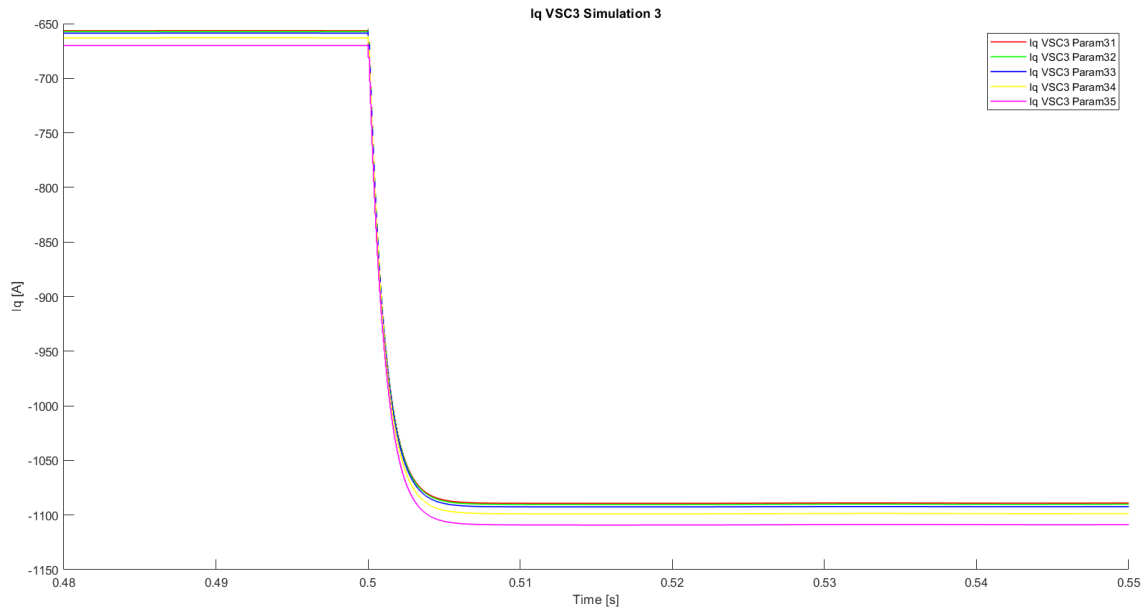


Figure 50: VSC3's i_q magnitude comparison during simulation 3.

The effects of q current magnitudes variations have the same origin as in the previous simulations. However, it is safe to assume that because q current magnitudes react in a more sensitive manner to the increase of cable length, V_{zq} magnitudes are equally prone to react. Due to cable's three placement, all converters display the same reaction when increasing the line length.

Secondly, d currents will be shown:

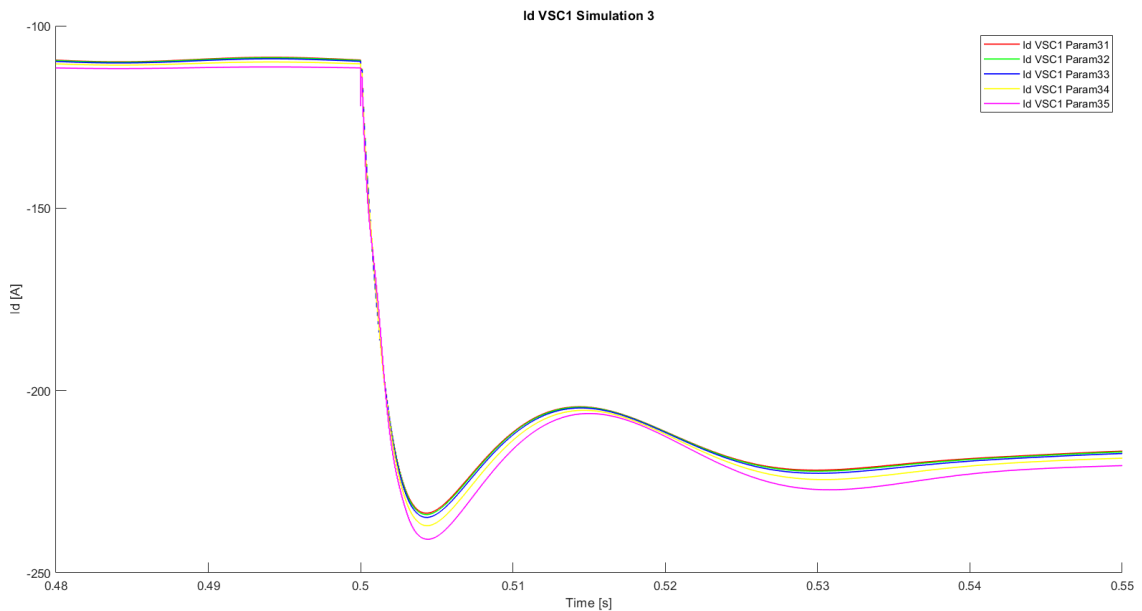


Figure 51: VSC1's i_q magnitude comparison during simulation 3.

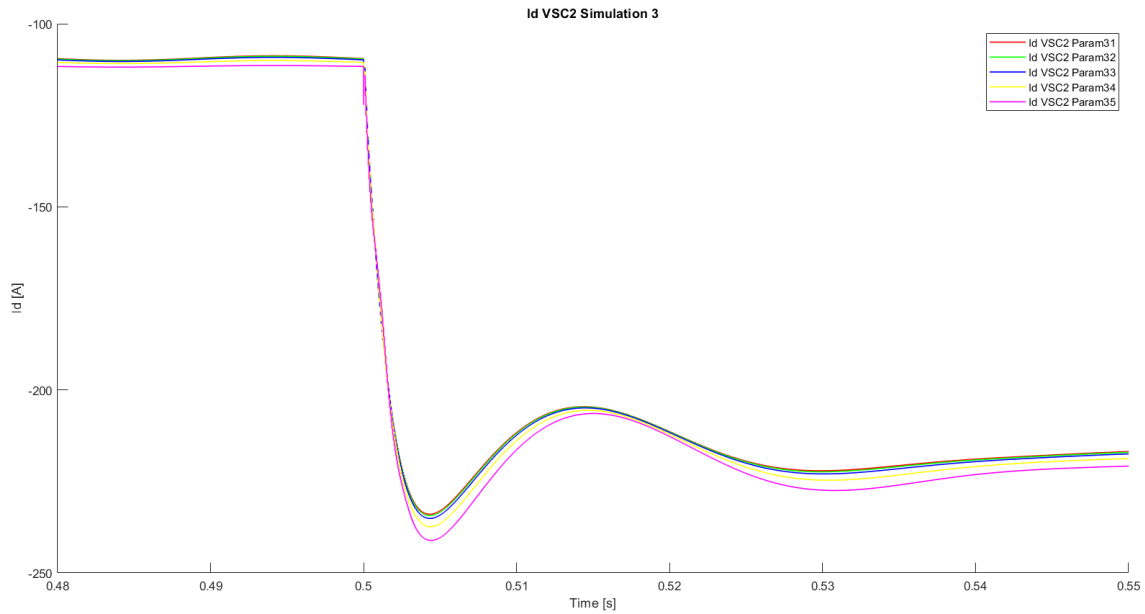


Figure 52: VSC2's i_q magnitude comparison during simulation 3.

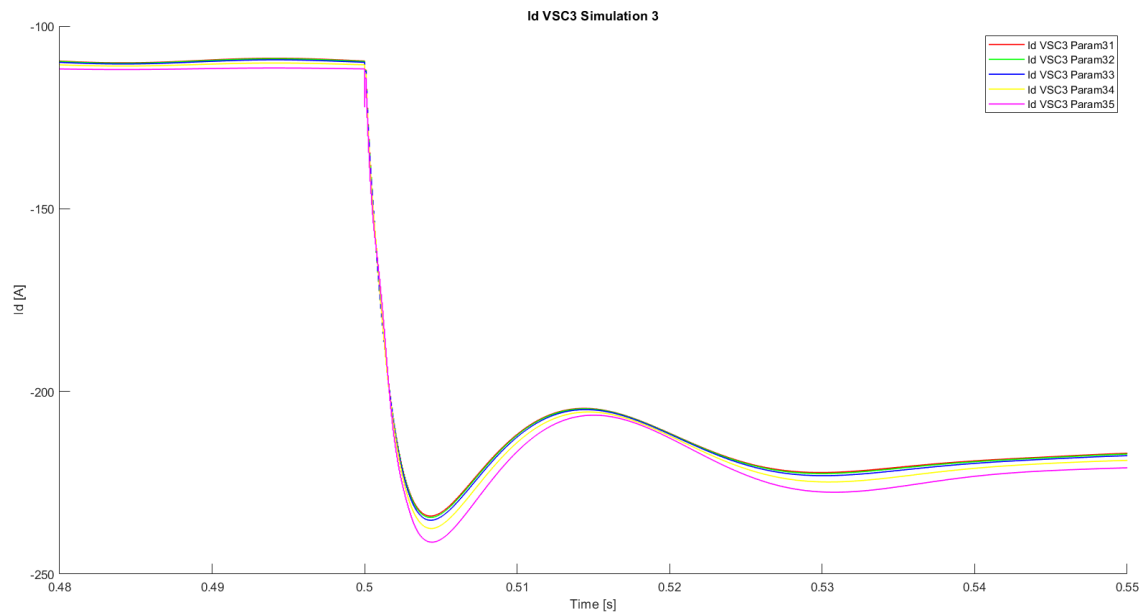


Figure 53: VSC3's i_d magnitude comparison during simulation 3.

Mirroring the behavior from the previous simulation, d currents from the converters present a brief oscillatory reaction at 0,5 seconds. Moreover, the overshoot values for all three converters display higher peak values as the distance increases compared to previous simulations.

Similarly to the data obtained from the preceding q currents, d quantities react in a more sensitive manner to an increase of cable's three length.

Regarding V_{zq} data, it was deemed unnecessary to present it due to the similarities obtained with the precedent simulations. However, an important evidence to underline

would be the fact that all three converters experience decrease in their LV side of the transformer as cable line 3 increases.

Finally, active power data will be shown:

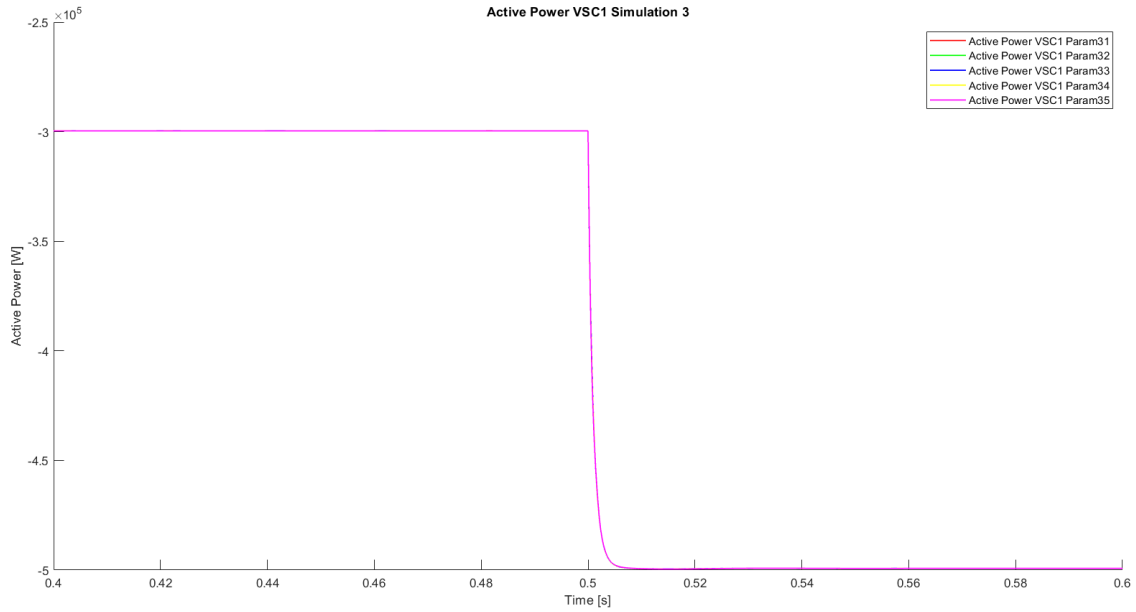


Figure 54: VSC1's active power magnitude comparison during simulation 3.

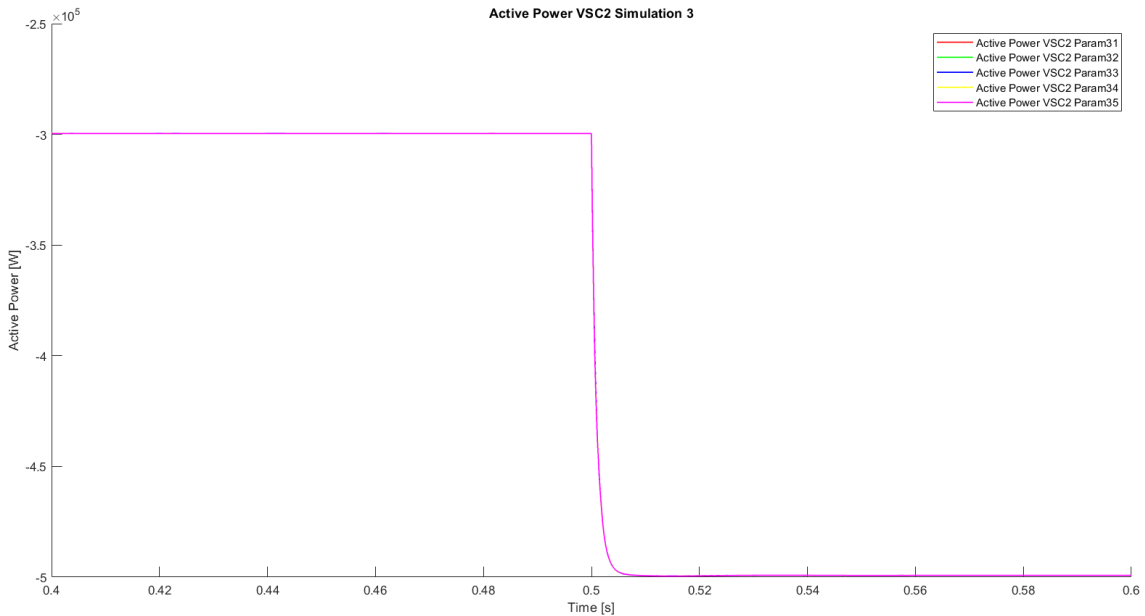


Figure 55: VSC2's active power magnitude comparison during simulation 3.

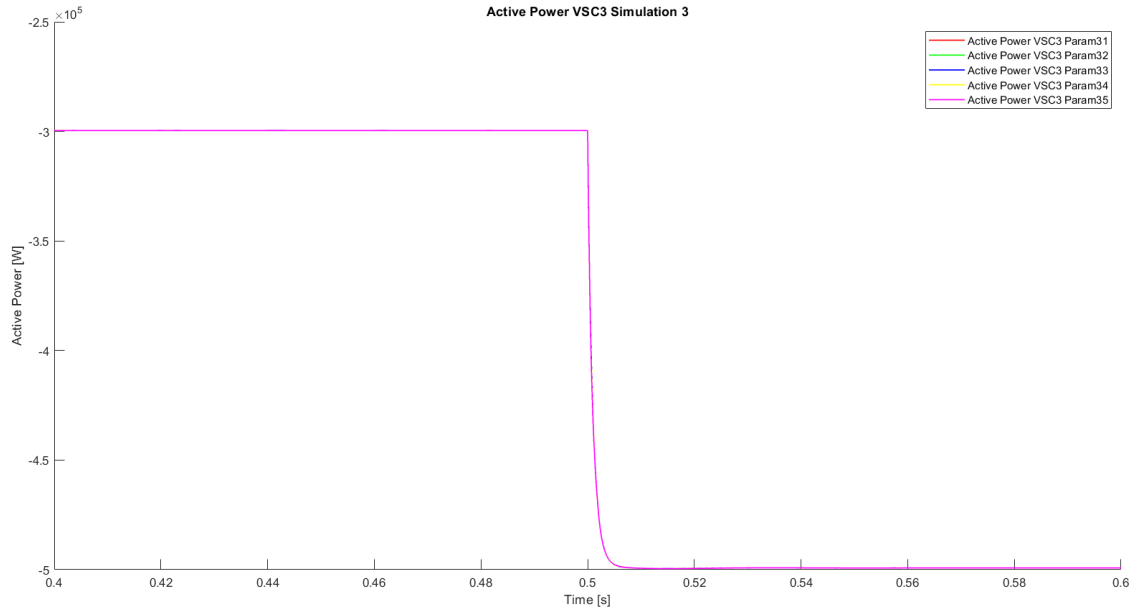


Figure 56: VSC3's active power magnitude comparison during simulation 3.

Mirroring the data obtained from the two precedent simulations, the active power supplied by the converter remains unaltered when varying cable's three length. The transition from one steady state to another mirrors the behavior obtained from simulation one.

9. CONCLUSION

After performing the mentioned data analysis, there are a few conclusions that can be obtained. Firstly, although the exact behavior (either increase or decrease) of current and voltage magnitudes in the qd domain cannot be strictly studied due to the nature of its obtention (see explanation in Chapter 8.4), the sensitivity of these magnitudes to the variation of each cable length can be studied. Therefore, a classification will now be made:

Converter	Simulation	Sensitivity
VSC 1	1	Low
VSC 2	1	Medium
VSC 3	1	Medium
VSC 1	2	Medium/Low
VSC 2	2	Medium/Low
VSC 3	2	Low
VSC 1	3	High
VSC 2	3	High
VSC 3	3	High

Table 7: Classification of the different cable lines in terms of sensitivity.

Therefore, it can be concluded that increasing cable's two length will bring the least variation in a voltage source converter's normal functioning. On the other hand, increasing the length of cable three will involve the biggest variation.

Finally, it can be concluded that the medium voltage cable length's variation does not affect the overall active and reactive power supplied by the converter.

10. ENVIRONMENTAL IMPACT

This project, alongside the other thousands of studies and researches performed all around the world are done behind on main reason: to aim for the reduction in the gross electricity production of non-renewable energies in favor of renewables. Therefore, it's safe to assume its effects are overall positive.

Regarding photovoltaic power plants, they do not pollute with harmful emissions which would contribute to the greenhouse effect. Moreover, their construction, if selected properly, is almost harmless. However, there are a few assessments that should be considered:

- Heritage: Trying not to destroy or have a major impact on a site's cultural heritage should be an important objective.
- Flora and Fauna: the assessment on the repercussions on both flora and fauna should be done.
- Agricultural Potential: As long as the terrain belongs to the company building the power plant, no assessment would be necessary. However, it is important to point out that an agricultural assessment is always encouraged.

However, as stated before, if selected appropriately, the construction of a photovoltaic power plant should cause no environmental harm.

Regarding the use of medium voltage cables, whether copper or aluminum would have been the material of use, they both are regarded as recyclable materials. Hence, no negative environmental impact is caused.

11. ECONOMIC STUDY

Regarding this project's budget, it will now be presented. Suffice it to say, this economic study is merely an approximation of real-life expenses should it have been carried out by an engineer from a company.

This project started on March 1st 2019 and was finished on September 10th 2019. Therefore, rounding it up, 6 months were spent on the project. Moreover, in terms of the engineer's salary, a total of 300 working hours will be computed as they equate to 12 ECTS.

Expenses	Price Per Unit	Units	Total Cost
Engineer Salary	25 €/hour	300 hours	7500 €
Office	850 €/month	6 months	5100 €
Equipment (Computer)	1000 €	1 unit	1000 €
Matlab License	69 €/year	6 months	34.5 €
Simscape Electrical Extension	20 €/year	6 months	10 €
Total			13644.5 €

Table 8: Display of the project's economic study.

12. BIBLIOGRAPHY

- [1] "IEA Data and Publications." [Online]. Available: <https://webstore.iea.org>.
- [2] "Agency, International Energy," 2019.
- [3] D. F. Birol, "Renewables 2018: Market analysis and forecast from 2018 to 2023.," 2018. [Online]. Available: <https://www.iea.org/renewables2018/>.
- [4] A. Karina Cabrera Tobar, "Large scale photovoltaic power plants," 2018.
- [5] C. McFadden, "How does a Solar Power Plant work?," 2018. [Online]. Available: <https://interestingengineering.com/how-does-a-solar-power-plant-work>.
- [6] M. (Penn S. U. Fedkin, "Main Components of Large PV Systems."
- [7] "Solar Cell Efficiency." [Online]. Available: https://en.wikipedia.org/wiki/Solar_cell_efficiency.
- [8] O. Gomis-bellmunt, "Active and reactive power control of grid connected distributed generation systems," pp. 1–35.
- [9] "Copper vs Aluminum Cables."
- [10] "Conductores de cobre vs Conductores de aluminio.," 2019. [Online]. Available: <https://4sproducts.com/conductores-de-cobre-vs-conductores-de-aluminio/>.
- [11] A. Urja, "Managing Solar Cables and Connectors," 2017. [Online]. Available: <https://mnre.gov.in/file-manager/akshay-urja/april-2017/Images/18-22.pdf>.
- [12] "6-36kV Medium Voltage Underground Power Cables."
- [13] "Short Circuit Fault Calculations." [Online]. Available: https://www.fs.fed.us/database/acad/elec/greenbook/10_shortcalc.pdf.
- [14] T. Assistance, "Solar Power Analysis and Design Specifications."